2008-12-02

Effect of KCNE1 and KCNE3 Accessory Subunits on KCNQ1 Potassium Channel Function: A Dissertation

Jessica Marie Rocheleau
University of Massachusetts Medical School

THE EFFECT OF KCNE1 AND KCNE3 ACCESSORY SUBUNITS ON KCNQ1 POTASSIUM CHANNEL FUNCTION

A Dissertation Presented

By

JESSICA MARIE ROCHELEAU

Submitted to the Faculty of the

University of Massachusetts Graduate School of Biomedical Sciences, Worcester

In partial fulfillment of the requirements for the degree of

DOCTOR OF PHILOSOPHY

December 2, 2008

Biochemistry and Molecular Pharmacology

THE EFFECT OF KCNE1 AND KCNE3 ACCESSORY SUBUNITS ON KCNQ1 POTASSIUM CHANNEL FUNCTION

A Dissertation Presented

By

JESSICA MARIE ROCHELEAU

The signatures of the Dissertation Defense Committee signify completion and approval as to style and content of the Dissertation

_____
William Kobertz, Ph.D., Thesis Advisor

_____
Dan Bolon, Ph.D., Member of Committee

_____
Lawrence Hayward, M.D., Ph.D., Member of Committee

_____
William Royer, Ph.D., Member of Committee

_____
Kenton Swartz, Ph.D., Member of Committee

The signature of the Chair of the Committee signifies that the written dissertation meets the requirements of the Dissertation Committee

_____
Anthony Carruthers, Ph.D., Chair of Committee

The signature of the Dean of the Graduate School of Biomedical Sciences signifies that the student has met all graduation requirements of the school

_____
Anthony Carruthers, Ph.D.,
Dean of the Graduate School of Biomedical Sciences

Program in Biochemistry and Molecular Pharmacology
December 2, 2008

DEDICATION

I dedicate this thesis in loving memory of my grandparents Pauline Vincent, Andre Vincent and Rodolph Rocheleau. And to my grandmother Corinne Rocheleau, I can't wait to see you at graduation!

ACKNOWLEDGEMENTS

First, I would like to acknowledge my thesis advisor, Bill Kobertz, for his endless support, encouragement, patience, and contagious enthusiasm. His guidance and insight propelled this work and helped me develop critical thinking, writing, and presentation skills. I am also grateful to the members of the Kobertz laboratory for assistance, advice, collaboration, and camaraderie. You made life in the lab a very enjoyable experience. In particular, Trevor Morin and Karen Mruk provided electrophysiology support and valuable manuscript editing, Steve Gage began the work for Chapter II of this thesis, Tuba Bas and Yuan Gao aided with biochemistry experiments, and Heidi Hafemann spent a rotation gathering preliminary calmodulin data.

I appreciate my committee members, Dan Bolon, Larry Hayward, Bill Royer, and committee chair, Tony Carruthers for their feedback and suggestions through the duration of my thesis research. Thanks to Kenton Swartz for serving as external committee member and for valuable conversations at Ion Channel Gordon Conferences.

Finally, I am indebted to my friends and family for their love, patience, and support during my graduate years. To my parents, Pierre and Michelle Rocheleau, thank you for always believing in me. I am grateful for my sister, Emily Rocheleau, my twin brother Matt Rocheleau and my sister-in-law Annie Mebane Rocheleau – your careers in politics and entertainment provide welcome distraction and keep me informed. Finally, to my boyfriend, Jason Rennie, thank you for your strength, love, and inspiration.

ABSTRACT

The KCNE1 and KCNE3 type I transmembrane-spanning β-subunits assemble with the KCNQ1 voltage-gated K^+ channel to afford membrane-embedded complexes with dramatically different properties. Assembly with KCNE1 produces the very slowly activating and deactivating I_{Ks} current that shapes the repolarization phase of cardiac action potentials. Genetic mutations in KCNQ1 or KCNE1 that reduce I_{Ks} current cause long QT syndrome and predispose affected individuals to potentially fatal cardiac arrhythmias. In contrast, complexes formed between KCNQ1 and KCNE3 produce rapidly activating and mostly voltage-independent currents, properties that are essential for function in K^+ recycling and Cl^- secretion in gastrointestinal epithelia.

This thesis addresses how these two homologous accessory peptides impart their distinctive effects on KCNQ1 channel gating by examining two important protein regions: 1) a conserved C-terminal motif in the β-subunits themselves, and 2) the voltage sensing domain of KCNQ1 channels.

Sequences in both the transmembrane domain and C-terminus of KCNE1 and KCNE3 have been identified as contributing to the divergent modulatory effects that these β-subunits exert. The homology of transmembrane-abutting C-terminal residues within the KCNE family and the presence of long QT-causing mutations in this region highlight its importance. A bipartite model of modulation was proposed that suggests the transmembrane domain of KCNE1 is passive, allowing the C-terminal domain to control modulation. Chapter II builds on this model by investigating the effect of mutating

specific amino acids in the KCNE1 C-terminal domain. Point mutants that produce 'high impact' perturbations in gating were shown to cluster in a periodic fashion, suggesting an alpha-helical secondary structure that is kinked by a conserved proline residue and interacts with the Q1 channel complex.

In Chapter III, the voltage sensing domain of Q1 channels is examined in the presence of either KCNE1 or KCNE3. To determine the influence of these two peptides on voltage sensing, the position of the S4 voltage sensor was monitored using cysteine accessibility experiments. In the slowly opening KCNQ1/KCNE1 complexes, voltage sensor activation appears to occur much faster than the onset of current, suggesting that slow channel activation is not due to slowly moving voltage sensors. KCNE3, on the other hand, shifts the voltage sensor equilibrium to favor the active state, producing open channels even at negative voltages.

Taken together, these findings provide mechanistic detail to illustrate how two homologous peptides radically alter the gating properties of the same K^+ channel and present a structural scaffold to map protein-protein interactions.

TABLE OF CONTENTS

LIST OF TABLES

LIST OF FIGURES

LIST OF SYMBOLS AND ABBREVIATIONS

α	Alpha
α-PI	Alpha-periodicity index
AKAP	A-kinase anchoring protein
β	Beta
CaM	Calmodulin
cAMP	adenosine 3',5'-cyclic monophosplate
Ci-VSP	*C. intestinalis* voltage-sensor-containing phosphatase
E1, E2, E3, E4, E5	KCNE1, KCNE2, KCNE3, KCNE4, KCNE5
FRET	Fluorescence resonance energy transfer
HA	hemagglutinin A
I_{Ks}	Slow cardiac potassium current
I_{Kr}	Rapid cardiac potassium current
K^+	Potassium
Kv channel	Voltage-gated potassium channel
LQTS	Long QT syndrome
MTS	Methanethiosulfonate
MTSET	[2-(trimethylammonium) ethyl] methanethiosulfonate
MTSES	(2-sulfonatoethyl) methanethiosulfonate
PIP_2	Phosphatidylinositol 4,5-bisphosphate
PKA	cAMP-dependent protein kinase
PP1	protein phosphatase 1
Q1	KCNQ1
TEVC	Two-electrode voltage clamp
VSD	Voltage sensing domain
WT	Wild-type

PREFACE

References to publications that represent the work contained within this thesis:

Rocheleau, J.M., S.D. Gage, and W.R. Kobertz. 2006. Secondary Structure of a KCNE Cytoplasmic Domain. *J. Gen. Physiol*. 128: 721-729

Rocheleau, J.M. and W.R. Kobertz. 2008. KCNE Peptides Differently affect Voltage Sensor Equilibrium and Equilibration Rates in KCNQ1 K^+ Channels. *J. Gen. Physiol.* 131:59-68

In Chapter II, Steve Gage generated mutant constructs and performed two-electrode voltage clamp recordings for positions F78-I82.

CHAPTER I: Introduction and Literature Survey

Voltage-gated K^+ (Kv) channels are critical for physiological processes that involve rapid response: propagating electrical signals throughout the nervous system, enabling cardiac, skeletal and smooth muscle contraction, and maintaining salt-water balance in gastrointestinal epithelia (Robbins, 2001; Bezanilla, 2006). This family of proteins functions in all kingdoms of life by providing an aqueous pore that opens and closes upon changes in membrane voltage. Potassium ions can then flow across the restrictive lipid bilayer and down their electrochemical gradient at a rate approaching that of simple diffusion. This remarkable speed is complemented by a very strong selectivity for K^+ over other monovalent cations.

Ion transport through Kv channels typically occurs in an outward direction – from the high K^+ environment of the cell interior to the outside of the cell where the K^+ concentration is much lower. In excitable cells, K^+ efflux repolarizes the membrane back to its typical resting potential of ~ -80 mV thereby terminating action potentials. The movement of potassium ions across the membrane generates a measurable current termed the ionic current. At any given voltage, the macroscopic ionic current from a population of channels depends on the single channel conductance, open probability and number of active channels at the cell surface.

Despite their diverse kinetic properties and tissue distribution, voltage-gated potassium channels share a common architecture. They are tetrameric assemblies of α-subunits (MacKinnon, 1991) whose amino- and carboxy- termini face the cytoplasmic

side of the membrane. Each α-subunit monomer contains six transmembrane-spanning segments (S1-S6) and the α-subunits probably assemble as dimers of dimers (Tu and Deutsch, 1999). Kv channels contain two essential domains: the voltage sensing domain (VSD) and the pore domain.

The Pore

The tetrameric arrangement of S5 and S6 helices forms the inverted tepee-shaped ion-conducting pore domain (Doyle et al., 1998). At the cytoplasmic face of the membrane, the S5 and S6 helices converge in a bundle crossing to form the gate that opens and closes to permit or restrict ion flow through the channel pore (Doyle et al., 1998). Ion flow can also be inhibited through a fast N-type inactivation process whereby a sequence of amino acids in the N-terminus of *Drosophila* Shaker-type K^+ channels binds the intracellular side of the channel (Hoshi et al., 1990; Zagotta et al., 1990). This finding, combined with studies showing that quaternary ammonium ions could block K^+ current through the pore from the intracellular side of the membrane and be trapped inside the pore suggested that the activation gate was located at the intracellular mouth of the pore (Armstrong, 1966; Armstrong, 1969; Armstrong, 1971). Further structure-function studies suggested that the C-terminus of S6 forms the gate (Choi et al., 1993; Liu et al., 1997; Holmgren et al., 1998; del Camino et al., 2000); this was complemented by comparing the crystal structures of bacterial K^+ channels in the open (MthK and KvAP) and closed (KcsA) conformations (Doyle et al., 1998; Jiang et al., 2002a; Jiang et al., 2003a). It is now understood that intracellular gate opening occurs via a hinge or kink in the pore-lining S6 helices. In prokaryotic K^+ channels, a conserved glycine in S6

forms a gating hinge (Jiang et al., 2002b; Jiang et al., 2003a); this is replaced by a Proline-X-Proline or Proline-X-Glycine motif (X is any amino acid) in eukaryotic channels that bends the S6 helix to open and close channels (Holmgren et al., 1998; del Camino et al., 2000; del Camino and Yellen, 2001; Webster et al., 2004). The closed KcsA crystal structure also revealed the reason for quaternary ammonium ion-trapping: the center of the pore opens up to a large water-filled cavity above the intracellular gate, roughly in the middle of the membrane. This effectively limits the distance that ions need to travel through the membrane to 12 Angstroms (Doyle et al., 1998).

Potassium selectivity is achieved by a sequence of amino acids at the narrowest part of the pore, close to the extracellular side of the membrane. The backbone carbonyl oxygen atoms in this 'selectivity filter' mimic the hydration shell of potassium ions in solution and the specific geometry of these carbonyl atoms permits K^+ ion flow while preventing proper coordination of smaller-radius Na^+ ions (Doyle et al., 1998; Zhou et al., 2001). Figure 1-1 shows the pore region and selectivity filter of KcsA, indicating the four K^+-coordinating positions. Electrostatic repulsion of adjacent K^+ ions in the selectivity filter ensures rapid conduction through the channel; however, at low K^+ concentrations, structural rearrangements of the selectivity filter can prevent ion conduction even if the intracellular gate is open (Zhou et al., 2001), a process called C-type inactivation (Lopez-Barneo et al., 1993).

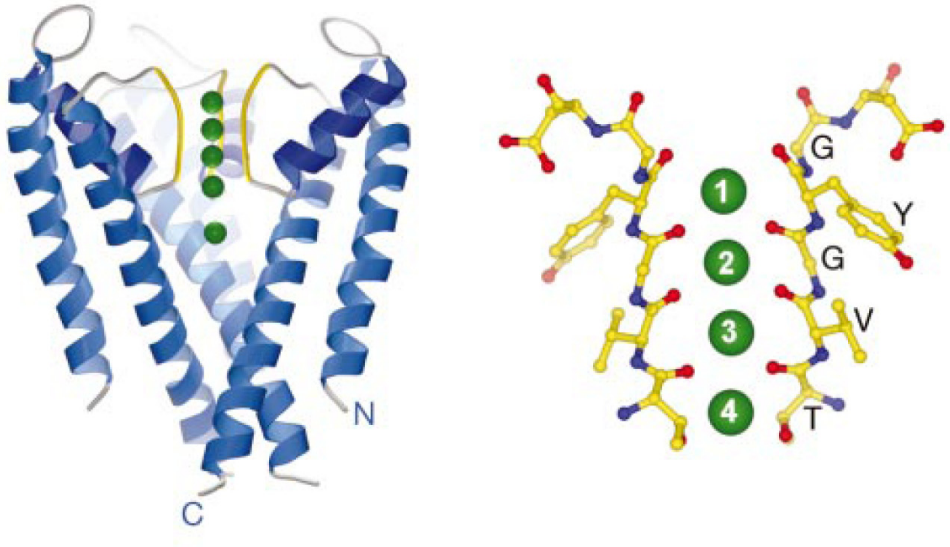

Figure 1-1 The pore and selectivity filter of the KcsA K^+ channel

(Left) Ribbon diagram showing three subunits of the bacterial KcsA K^+ channel crystal structure (front subunit omitted for clarity). The selectivity filter is depicted in yellow, and potassium ions binding four sites in the selectivity filter and one site in the water-filled cavity are indicated in green.

(Right) Close-up view of residues from two subunits forming the selectivity filter (front and back subunits not depicted). Backbone carbonyl atoms form four K^+ ion coordination sites. Figure 1-1 is from (Morais-Cabral et al., 2001).

The Voltage Sensing Domain

The first four transmembrane segments (S1-S4) sit on the periphery of the central pore and comprise the voltage sensing domain (VSD). Since voltage-gated channels are defined by their strong dependence on changes in membrane voltage to open (activate) and close (deactivate), Hodgkin and Huxley proposed that a 'gating particle' within the channel acts as a voltage sensor (Hodgkin and Huxley, 1952). The repeating pattern of positively charged arginine and lysine residues at every third position in the S4 transmembrane helix pointed to this segment as the possible gating particle, or voltage sensor. When the cell interior is depolarized, the positively charged S4 helices move out toward the cell exterior (Larsson et al., 1996; Yang et al., 1996). This movement in itself creates a very small, transient 'gating current' that can be measured if enough channels are expressed at the cell surface and if the ionic current is blocked (Armstrong and Bezanilla, 1973; Armstrong and Bezanilla, 1974). Gating current measurements have revealed that in a single Shaker Kv channel, ~ 13 electron charge units are displaced upon channel opening, or ~ 3 per subunit (Aggarwal and MacKinnon, 1996; Seoh et al., 1996). Neutralization of S4 charges substantially decreases the gating charge, indicating that the four most N-terminal arginines translocate the majority of this charge (Aggarwal and MacKinnon, 1996). The distance over which voltage sensors travel during activation and the chemical environment surrounding S4 charges has been the subject of intense debate.

Models of Voltage sensing

The crystal structures of three VSD-containing K^+ channels show that the S3 and S4 subunits form an antiparallel helical domain termed the voltage sensor paddle (Jiang et al., 2003a; Long et al., 2005a; Long et al., 2007). Accessibility studies performed with methanethiosulfonate (MTS) reagents (Larsson et al., 1996; Yang et al., 1996) and more recent probing with avidin capture of tethered biotin (Jiang et al., 2003b; Ruta et al., 2003) suggest that upon depolarization, the S4 helices traverse 15-20 Å through the membrane. Other approaches suggest a smaller translocation no more than the outer half of the lipid bilayer (Phillips et al., 2005) or $\sim$4 Å through a more focused electric field (Ahern and Horn, 2005). Finally, fluorescence resonance energy transfer experiments invoke comparatively tiny vertical displacements of 2 Å or less (Chanda et al., 2005; Posson et al., 2005). These models essentially depend on the degree of electric field focusing across the membrane. A smaller, more focused electric field requires smaller S4 movements to generate the gating charge whereas a membrane electric field spread across a greater distance requires larger motions (Tombola et al., 2006).

There has also been some discrepancy concerning whether the environment surrounding S4 arginines consists of protein, water, lipid, or a mixture of these. It seems energetically unfavorable for positively charged guanidinium groups to be buried in the low-dielectric lipid bilayer. Indeed, the accessibility of S4 residues to water-soluble reagents suggests that the gating charge arginines may be protected by water-filled crevices (Larsson et al., 1996; Yang et al., 1996; Cha et al., 1999; Starace and Bezanilla, 2004). Additionally, the finding that an arginine to histidine substitution in Shaker's S4

creates a proton pore in the VSD supports an aqueous – or at least ion-friendly – voltage sensor environment (Starace et al., 1997). Finally, acidic amino acids in S1 and S2 are postulated to form salt bridges with some of the basic S4 gating charges (Seoh et al., 1996). Two recent crystal structures of mammalian Kv channels confirm that the third and fourth arginines are stabilized by salt bridge interactions with acidic amino acids on S1 and S2 (Long et al., 2005a; Long et al., 2007). The more N-terminal gating charge arginines are on a lipid-facing surface and may extend to face phospholipid head groups.

Coupling Voltage Sensing to Gating

It is now accepted that membrane depolarization causes the outward displacement of voltage sensor helices, which triggers intracellular gate opening and allows ion conduction through the channel. The Kv1.2 crystal structure presents an electromechanical mechanism to describe the tight coupling between voltage sensor activation and gate opening (Long et al., 2005b). The VSD of one subunit surrounds the pore forming helices of an adjacent subunit, so that the S4-S5 linker – a helical domain that lies parallel to the membrane connecting the VSD and pore – travels underneath the neighboring subunit (Fig 1-2). When voltage sensors are activated, the S4-S5 linkers widen the ion conduction pathway to open the channel. Upon hyperpolarization, voltage sensors return to their resting state, the S4-S5 linkers clamp down, and compress the C-terminal region of the S6 gate to close the pore and prevent ions from entering.

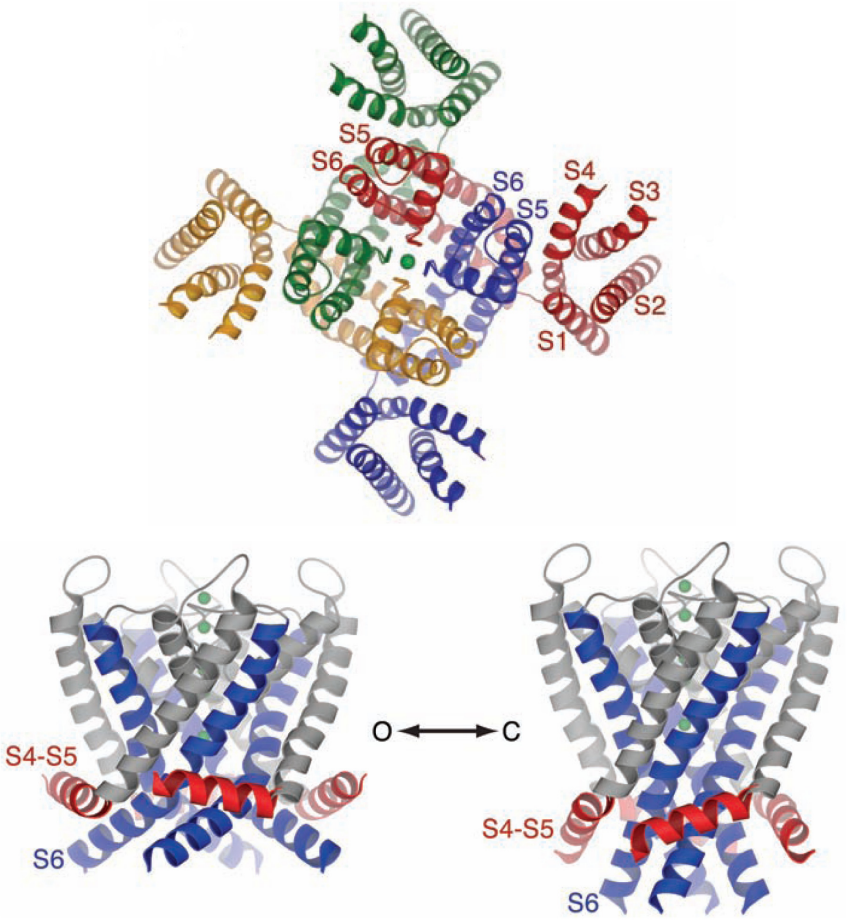

Figure 1-2 Proposed mechanism of voltage-dependent gating

(Top) Ribbon diagram showing the Kv1.2 crystal structure top-down, from the extracellular side of the membrane. Each subunit is presented in a different color (red, blue, gold, green), and helical segments are labeled S1-S6. A single potassium ion is modeled in the center of the pore.

(Bottom) Ribbon diagram side-view of the open conformation (left) and hypothetical closed conformation (right) of the Kv1.2 pore-forming subunits. S4-S5 linkers are in red, S5 helices in grey and S6 helices in blue. Green spheres show potassium ions modeled in the pore region. Figure 1-2 is from (Long et al., 2005b).

This coupling mechanism is supported by studies that transplanted a VSD onto an otherwise voltage-independent channel. For proper voltage-dependent function, these channels required both the S4-S5 linker region and a C-terminal portion of S6 (Lu et al., 2001; Lu et al., 2002). Point mutations in the pore region highlight the localized region of interaction and the relative independence of voltage sensing domains (Li-Smerin et al., 2000b; Soler-Llavina et al., 2006). Moreover, two proteins were recently identified with VSDs that function completely independently of pore domains: The *C. intestinalis* voltage-sensor-containing phosphatase (Ci-VSP) contains a VSD coupled to a phosphatase that forms the only known voltage-dependent enzyme (Murata et al., 2005), and the Hv1 protein is a VSD that, by itself, serves as a voltage-dependent proton pore (Ramsey et al., 2006; Sasaki et al., 2006). Despite the independence of voltage-sensing domains and the relatively small interacting region with the pore, most Kv channels show strong coupling between domains. Given that the probability of gate opening at hyperpolarized potentials is extremely low (Islas and Sigworth, 1999), the coupling mechanism demands that voltage sensors be in the active conformation for the gate to open.

KCNQ1 K^+ Channels

KCNQ1 (Q1), a member of the Kv7 family of voltage-gated potassium channels, is the subject of this thesis. Q1 shares the standard Kv topology of α-subunits containing six transmembrane helices that tetramerize to form a K^+-selective pore with four surrounding VSDs (Wang et al., 1996). Despite the scarcity of structural data describing Q1, sequence homology predicts a similar structural scaffold to Kv1.2. However, the C-

terminus of Q1 channels is much larger than in other Kv channels, an important feature that allows this region to act as a scaffold for many intracellular signaling proteins. Q1 channels also activate slower than other Kv channels and have a very small single channel conductance between 0.7 and 4 pS (Pusch, 1998; Sesti and Goldstein, 1998; Yang and Sigworth, 1998). This may be explained by the fact that Q1 has fewer positively charged residues in each S4 segment, as demonstrated in the sequence alignment in Fig 1-3 (Panaghie and Abbott, 2007). Unlike many Kv channels, including the other four members of the Kv7 family, Q1 is not expressed in the nervous system at all, but is primarily found in cardiac and epithelial tissues (Wang et al., 1996; Yang et al., 1997). Voltage-dependent activation of Q1 channels is accompanied by a delayed inactivation process that, unlike classic C-type inactivation, occurs independent of extracellular K^+ concentration (Pusch et al., 1998). Delayed rectifying currents arising from Q1 channels exogenously expressed in *Xenopus* oocytes or cultured cells do not match any physiologically observed currents. Rather, Q1 assembles with all five members of the KCNE family of β-subunits (E1-E5), which cause this otherwise voltage-dependent channel to adopt a variety of unique gating properties and pharmacologic sensitivities depending on the KCNE β-subunit with which it assembles (Barhanin et al., 1996; Sanguinetti et al., 1996; Schroeder et al., 2000; Tinel et al., 2000; Angelo et al., 2002; Grunnet et al., 2002).

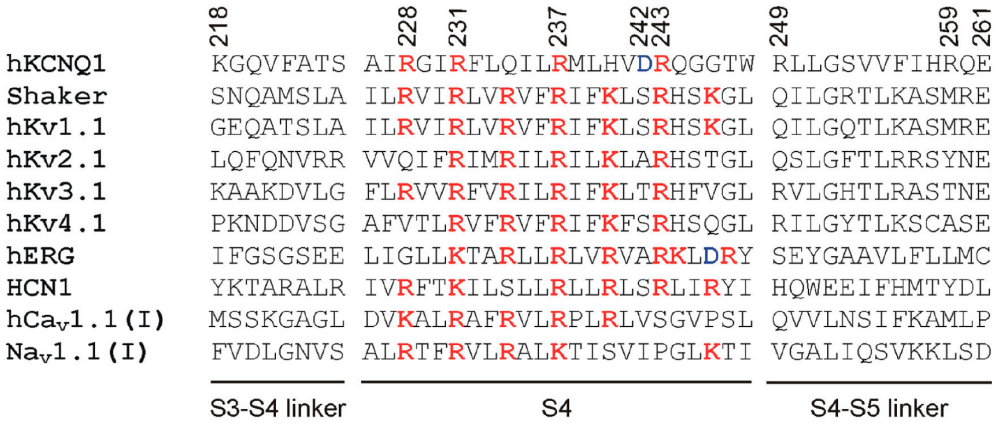

Figure 1-3 Sequence alignment for the S4 region in a variety of human ion channels

Amino acid sequence of the S3-S4 linker, S4 and S4-S5 linker regions of human ion channel subunits. Positively charged arginine (R) or Lysine (K) residues are presented in red. Figure 1-3 is from (Panaghie and Abbott, 2007).

KCNE β-subunits

KCNE β-subunits are small (103-177 amino acids), single transmembrane spanning peptides that form stable complexes with a variety of Kv channels and modulate their function (McCrossan and Abbott, 2004). These mostly α-helical peptides (Kang et al., 2008) extend their C-termini into the cytosol; their extracellular N-termini contain conserved N-linked glycosylation sites that have been useful for following KCNE trafficking through the secretory pathway (Chandrasekhar et al., 2006). The founding member of this family, KCNE1 (E1), assembles with Q1 in the heart and inner ear to generate an extremely slowly activating and deactivating delayed rectifying complex (Barhanin et al., 1996; Sanguinetti et al., 1996). When KCNE2 (E2) is expressed with Q1, the currents produced are voltage-independent, with diminished amplitude compared to Q1 channels expressed alone (Tinel et al., 2000). Q1/E2 complexes are present in parietal cells of the stomach, where they are required for gastric acid secretion (Roepke et al., 2006). E2 also assembles with another Kv channel, Kv11 (HERG) to form the rapidly activating I_{Kr} current in heart (Abbott et al., 1999). Complexes formed by Q1 and KCNE3 (E3) activate almost instantaneously, conduct current at all measurable voltages, and co-localize in colonic crypt cells to recycle potassium and mediate cAMP-stimulated chloride secretion (Schroeder et al., 2000). E3 also assembles with the Kv3.4 channel in skeletal muscle, where mutations in E3 are associated with periodic paralysis (Abbott et al., 2001). In contrast, E4 acts as an inhibitory subunit to Q1 (Grunnet et al., 2002), and E5 radically right-shifts the voltage activation of Q1 channels (Angelo et al., 2002). While the biological roles of Q1/E4 and Q1/E5 complexes are still unclear, messenger

RNA encoding all five KCNE peptides has been detected in human heart, suggesting that a balance of KCNEs may be important for cardiac potassium channel function (Bendahhou et al., 2005; Lundquist et al., 2005). Indeed, it was recently shown that different KCNE peptides can assemble with the same Q1 channel in a heteromeric complex, suggesting an additional level of K^+ channel diversification by β-subunits (Morin and Kobertz, 2007; Manderfield and George, 2008).

Long QT Syndrome

The physiological importance of Q1/KCNE complexes is highlighted by the fact that mutations in both subunits cause disease. The slowly activating I_{Ks} current generated by Q1/E1 complexes in the heart contributes to a healthy heart rhythm by shaping the repolarization phase of cardiac action potentials. The precise timing of action potentials is critical, and is reflected in the interval between Q and T waves on an electrocardiogram (ECG). Mutations in Q1 or E1 that suppress channel function or prevent proper trafficking to the plasma membrane diminish the I_{Ks} current and impair repolarization, thereby prolonging the duration of cardiac action potentials and the corresponding QT interval of the ECG (Splawski et al., 1997; Bianchi et al., 1999; Splawski et al., 2000; Wilson et al., 2005). This hereditary form of long QT syndrome (LQTS) affects 1 in 5000 individuals, causing seizures, sudden loss of consciousness (syncope), ventricular arrhythmias (torsades de pointes), and can even lead to sudden death (Kass and Moss, 2003). Romano-Ward syndrome is the more common form of this cardiac disorder and is inherited as an autosomal dominant trait (Romano et al., 1963; Ward, 1964). The much rarer Jervell and Lange-Nielson syndrome is inherited as an autosomal recessive disesase;

homozygotes show more severe cardiac abnormalities, have a higher risk of sudden death, and the QT prolongation is accompanied by congenital bilateral deafness (Jervell and Lange-Nielsen, 1957).

Why does a dysfunctional cardiac K^+ channel cause deafness? In addition to expression in the heart, Q1/E1 complexes are the sole carrier of K^+ secretion across the apical membranes of vestibular dark cells and strial marginal cells in the inner ear (Wangemann et al., 1995). Voltage-dependent Q1/E1 complexes are always open at the apical membrane potential of ~10 mV and the resultant current contributes to endolymph secretion required for normal hearing. When both copies of Q1 or E1 contain loss-of-function mutations, the lack of functional currents disrupts K^+ recycling and endolymph homeostasis, causing neural deafness. The severity of disease may also depend on the specific site and type of mutation. For example, two mutations in the C-terminus of E1 cause LQTS: S74L and D76N (Splawski et al., 1997). Whereas S74L shifts the voltage dependence of activation to more positive voltages causing a significant reduction in I_{Ks} current, D76N completely abolishes channel function even though channels harboring this mutation successfully reach the plasma membrane (Wang and Goldstein, 1995). Mutations causing LQTS have now been identified in the N-terminus, transmembrane domain, and C-terminus of E1 as well as throughout the pore-forming Q1 subunit (Splawski et al., 2000).

Q1/E1 channels in human heart are also regulated by sympathetic nervous system stimulation since cardiac arrhythmias in patients carrying long QT mutations in Q1 or E1 are sometimes precipitated by exercise or startling (Schwartz et al., 2001). During

exercise or a fight-or-flight response, neurons release norepinepherine, which binds to β-adrenergic receptors and activates the cAMP-dependent protein kinase A (PKA) signaling pathway to increase heart rate and shorten cardiac action potential duration (Kass and Wiegers, 1982).

Intracellular Regulation

The connection between β-adrenergic signaling and Q1/E1 channel regulation revealed that Q1/E1 channels are part of a much larger macromolecular signaling complex (Marx et al., 2002). In response to β-adrenergic signaling, PKA and protein phosphatase 1 (PP1) are recruited to regulate Q1 phosphorylation at serine 27 by the A-kinase anchoring protein (AKAP), yotiao. Yotiao binds a leucine zipper motif in the large C-terminal domain of Q1. Phosphorylated channels generate increased I_{Ks} current and long QT mutations in the C-terminal leucine zipper motif prevent yotiao binding, PKA recruitment, and subsequent Q1 phosphorylation, thereby ablating cAMP-mediated regulation of the channel (Marx et al., 2002). Two other long QT mutations in the E1 C-terminus (D76N and W87R) also disrupt this functional regulation (Kurokawa et al., 2003). Q1/E1 channel complexes may also connect to the cytoskeletal network via interactions with β-tubulin, since disruption of microtubules diminishes I_{Ks} response to PKA-dependent stimulation (Nicolas et al., 2008).

Given that intracellular calcium alters the amplitude of I_{Ks} currents, calmodulin was proposed to bind and regulate Q1. Assembly with calmodulin underlies the calcium sensitivity of Q1/E1 complexes, and its constitutive interaction with the Q1 C-terminal

IQ motifs – even in the absence of calcium – promotes solubility of this domain and is required for efficient channel delivery to the cell surface (Ghosh et al., 2006; Shamgar et al., 2006). Accordingly, long QT mutants in the Q1 C-terminus that impair calmodulin binding result in reduced current amplitude. Assembly between calmodulin and Q1 can be disrupted by phosphatidylinositol 4,5-bisphosphate (PIP_2) interaction with the same Q1 domain, which activates Q1/E1 channels by left-shifting the voltage-dependence of activation (Loussouarn and Escande, 2003; Kwon et al., 2007).

Secondary structure predictions indicate that the Q1 C-terminus possesses four conserved helical regions (Yus-Najera et al., 2002). The first two contain the calmodulin and PIP_2 binding domains, while the second two helices form coiled coil domains that mediate subunit tetramerization. Unlike other members of the KCNQ family that contribute to neuronal M-currents and can form heterotetrameric channels, Q1 forms homotetramers exclusively, a property attributed to the longer coiled coil region (Howard et al., 2007; Wiener et al., 2008).

The importance of the Q1 C-terminus as a multi-tiered scaffold involved in assembly, subunit specificity, trafficking, and regulation by a number of intracellular signaling proteins highlights the complexity of regulation that this channel experiences. As mentioned above, functional diversity is also achieved by Q1 assembly with a variety of β-subunits that fine-tune its electrical output.

Q1/E1 and Q1/E3 assembly, interaction, and modulation

This thesis addresses the nature of Q1 modulation by two different KCNE β-subunits: E1 and E3. Whereas Q1/E1 complexes generate very slowly activating,

voltage-dependent currents, Q1/E3 complexes activate rapidly and are mostly voltage-independent, producing current at all measurable voltages.

The exact location of KCNE peptides within the Q1 channel is still debated. Although E1 has been suggested to line the Q1 ion-conducting pore (Tai and Goldstein, 1998; Chen et al., 2003b), every K^+ channel crystal structure demonstrates that the pore region, and the selectivity filter in particular, is too small to surround any number of β-subunits. Accumulating evidence demonstrates physical interaction between both E1 and E3 peptides and the S6 region of Q1 (Tapper and George, 2001; Melman et al., 2004; Panaghie et al., 2006), and the new model proposes a permissive pore conformation that allows an extended binding surface for KCNE peptides, which may each bind the channel in slightly different ways (Melman et al., 2004). A recent report also puts to rest the longstanding dispute over how many β-subunits are present in a single channel complex. Two, four, or a mixed number of KCNE subunits per complex have all been suggested (Wang and Goldstein, 1995; Wang et al., 1998; Chen et al., 2003a), however a tethered-blocker approach conclusively counted two E1 β-subunits in functioning Q1/E1 complexes (Morin and Kobertz, 2008). This study also provides some distance measurements that constrain the location of KCNEs within the Q1 complex. Since the shortest tethering linker used was 20 Å in length, the N-terminus of E1 probably resides approximately 20 Å from the pore.

The nature of Q1 modulation by E1 and E3 has also been investigated in some detail. Progressive truncation of the E1 C-terminus removes the characteristic slow activation of Q1/E1 complexes without preventing coassembly, suggesting that a stretch

of C-terminal residues abutting the transmembrane domain is required for E1's modulatory effect (Takumi et al., 1991; Tapper and George, 2000). In contrast, chimeras that mix and match different homologous domains in E1 and E3 suggest that a triplet of amino acids in the transmembrane region controls modulation. When these residues are swapped from E1 to E3 and vice versa, they confer the identity of the donor to the recipient. For example, when residues FTL from E1 replace the corresponding TVG residues in E3, the resulting current is slowly activating and voltage dependent, reminiscent of Q1/E1 currents (Melman et al., 2001). Melman and colleagues further postulated that a simple hydroxyl group on the central residue of this 'activation triplet' controls the specificity of gating and that the C-terminus merely mediates specific β-subunit positioning in the channel complex (Melman et al., 2002). These divergent ideas were reconciled with a bipartite model of Q1 modulation by E1 and E3 (Gage and Kobertz, 2004). This model explains that the transmembrane and C-terminal domains participate in both assembly and modulation; however, the transmembrane sequence is either active or passive in generating voltage-independent currents (basal activation). The active E3 transmembrane domain dominates any C-terminal contribution to modulation resulting in a large amount of basal activation. The E1 transmembrane domain is passive, uncovering C-terminal modulation of Q1 that produces slowly activating and deactivating currents.

Does the E1 C-terminus directly interact with Q1 to control slow gating? Chapter II of this thesis expands on the bipartite model by identifying individual amino acids in the E1 C-terminus that are critical for modulation of Q1. Given the sequence

conservation of transmembrane-abutting C-terminal residues in KCNE peptides and the presence of long QT-causing mutations in this domain, detecting key interacting residues and uncovering secondary structural elements would have important implications for the structure and function of the KCNE family as well as possible LQTS therapies. This work describes the application of perturbation mutagenesis and helical analysis to answer this question.

Further questions remain concerning possible interactions between KCNE β-subunits and the voltage sensing domain. Although both E1 and E3 have been shown to interact with the pore region, the extremely slow Q1/E1 currents and voltage-independent Q1/E3 currents suggest that assembly of these β-subunits with Q1 may alter voltage sensor equilibrium. Abbott and coworkers suggested that the paucity of charge in Q1's S4 makes it uniquely sensitive to the modulatory effects of E1 and E3, which do not affect other Kv channels as drastically (Panaghie and Abbott, 2007).

To generate slowly activating currents, it's possible that E1 either slows the equilibration rate of Q1 voltage sensors or slows the opening of the activation gate. For voltage-independent currents at negative voltages, E3 either shifts voltage sensors to favor the active state or uncouples voltage sensor movement from gate opening. Chapter III of this thesis uses MTS-accessibility analysis to assess the equilibrium of voltage sensors in Q1/E1 and Q1/E3 to directly distinguish these possibilities.

CHAPTER II: Secondary Structure of a KCNE Cytoplasmic Domain

Abstract

KCNE peptides contain a conserved C-terminal cytoplasmic domain that abuts the transmembrane segment. In E1, this region is required for modulation of Q1 K^+ channels to afford the slowly activating cardiac I_{Ks} current. This chapter describes the application of perturbation mutagenesis to determine whether the E1 C-terminus possesses any secondary structure and to identify the E1 residues that face the Q1 channel complex.

A series of alanine and leucine point mutations were introduced into the E1 C-terminus and standard activation curve analysis was used to calculate the free energy of channel opening. Helical periodicity analysis of these mutation-induced perturbations defined the E1 C-terminus as α-helical when split in half at a conserved proline residue. This helical rendering assigns all known long QT mutations in the E1 C-terminal domain as protein-facing. The identification of secondary structure within the E1 C-terminal domain provides a structural scaffold to map protein-protein interactions with the pore-forming Q1 subunit as well as the cytoplasmic regulatory proteins anchored to Q1/KCNE complexes.

Introduction

KCNE type I transmembrane peptides are a class of membrane-embedded β-subunits that assemble with and modulate the function of voltage-gated K^+ channels (McCrossan and Abbott, 2004). The physiological importance of these small (100 -150 aa) β-subunits on K^+ channel function is underscored by the genetic mutations in E1 and E2 that cause abnormalities in the cardiac rhythm (Splawski et al., 2000). Outside of the heart, mutations in E1 also cause endolymphatic collapse in the developing ear and a C-terminal mutation in E3 has been implicated in periodic paralysis since it alters Kv3.4 channel function (Letts et al., 2000; Abbott et al., 2001). All five KCNE peptides assemble with and differentially modulate Q1 K^+ channels (McCrossan and Abbott, 2004). Q1/E1 complexes produce the slowly activating and deactivating cardiac I_{Ks} current whereas Q1 assembly with either E2 or E3 gives rise to constitutively conducting complexes that rapidly activate and deactivate. Complexes with E4 and E5 slow the activation kinetics of Q1 channels similarly to E1; however, co-assembly with these more recently discovered KCNEs results in K^+ channel complexes that conduct only at extremely depolarizing potentials. Q1/KCNE complex gating is also modulated by several intracellular proteins. Calmodulin, PKA, protein phosphatase I (PP1), and A-kinase anchoring proteins (AKAPs) are all cytoplasmic proteins that interact with membrane-embedded Q1/KCNE complexes (Marx et al., 2002; Kurokawa et al., 2003; Shamgar et al., 2006).

Although KCNE peptides modulate Q1 function differently, four KCNE peptides share a conserved cytoplasmic sequence of ~ 20 amino acids adjacent to the transmembrane domain. Structure-function studies with E1 have shown that this domain is required for Q1 channel modulation (Takumi et al., 1991; Tapper and George, 2000). Moreover, one-third of the known genetic missense point mutations in E1 that cause long QT syndrome reside in this cytoplasmic region (Splawski et al., 2000; Schulze-Bahr et al., 2001; Ma et al., 2003; Lai et al., 2005; Napolitano et al., 2005).

This chapter describes the use of perturbation mutagenesis to determine whether the E1 cytoplasmic domain possesses any secondary structure and to identify residues that interact with Q1 channels. Alanine and tryptophan scanning has been previously used to examine the secondary structure and protein-facing residues of both soluble and membrane-embedded domains of voltage-gated K^+ channels (Monks et al., 1999; Hong and Miller, 2000; Li-Smerin et al., 2000a; Li-Smerin et al., 2000b). Using alanine and leucine mutagenesis, two distinct classes of E1 mutants were identified: those that strongly shift the voltage-dependence of activation favoring the closed state, and those that resemble the wild type complex. Periodicity analysis of this data reveals that the cytoplasmic C-terminal domain of E1 is helical when broken into two segments separated by a proline residue. This suggests that either the E1 C-terminus is kinked, or it experiences two different protein environments above and below this junction point. Moreover, this helical rendering defines all known long QT mutations in this region as protein-facing. Given that this domain is conserved in all but one of the known KCNE peptides, the E1 results predict that E2, E3 and E5 will possess a domain with similar

structure when associated with Q1 channel subunits. In total, these results provide a structural motif from which to interpret the link between Q1/KCNE gating and intracellular regulation.

Materials and Methods

Mutagenesis and in vitro transcription: Q1 and E1 were subcloned into vectors containing the 5' and 3' UTRs from the *Xenopus* β-globin gene for optimal protein expression. Single point mutations were introduced into human E1 using Quickchange site-directed mutagenesis (Strategene) and confirmed by DNA sequencing. For all surface luminometry experiments, the hemagglutinin A (HA) tag, YPYDVPDYA, was incorporated into the N-terminus of E1 between residues 22 and 23 (Abbott et al., 2001). The cDNA plasmids were linearized by MluI digestion, and cRNA was synthesized by run-off transcription using SP6 or T7 RNA polymerase (Promega).

Electrophysiology: Oocytes were surgically removed from *Xenopus laevis* and defolliculated using 2 mg/mL collagenase (Worthington Biochemical Corp.) in OR2 containing (mM): 82.5 NaCl, 2.5 KCl, 1 $MgCl_2$, 5 HEPES, pH 7.4 for 75-90 min. Isolated oocytes were rinsed with and stored in ND96 bathing solution (ND96B) containing (mM): 96 NaCl, 2 KCl, 1.8 $CaCl_2$, 1 $MgCl_2$, 5 HEPES, 50 μg/mL gentamicin (Sigma-Aldrich), pH 7.4 at 18°C. Approximately 24h after extraction, oocytes were microinjected with 27.6 nL total volume of cRNA containing Q1 (7.5 ng/oocyte) and E1 (3.75 ng/oocyte). After 3–6 days, currents were recorded using Warner Instrument OC-725C two-electrode voltage clamp (TEVC) and the data were acquired with Digidata 1322A using pClamp 8 or 9 (Axon Instruments). Electrodes were filled with 3 M KCl, 5 mM EGTA, 10 mM HEPES, pH 7.6, and had resistance between 0.2 and 1.0 MΩ. For

each experiment, oocytes were held at – 80 mV in ND96 (in mM): 96 NaCl, 2 KCl, 0.3 $CaCl_2$, 1 $MgCl_2$, 5 HEPES, pH 7.4, and pulsed to a command potential of 40 mV. Oocytes injected with Q1 and wild type or mutant E1 RNA were only recorded from if a pulse to 40 mV produced current greater than 1 μA to ensure that currents were coming from exogenously injected channel complexes. Tail currents for activation curves were measured in KD98 (in mM): 98 KCl, 0.3 $CaCl_2$, 1 $MgCl_2$, 5 HEPES, pH 7.4. Oocytes were held at – 80 mV and the tail current protocol was a series of 4 s test pulses to potentials between –100 and + 60 mV in 10 mV increments.

Data Analysis: The amplitude of tail currents was measured 6 ms after repolarization to – 80 mV and plotted versus the depolarized potential to produce activation curves for wild type and mutant E1 channel complexes. Activation curves were fit to a Boltzmann function, $I/I_{max} = A2 + (A1 - A2) / (1 + e^{(V - V1/2)*(-zF/RT)})$, where I/I_{max} is the normalized tail current amplitude, $V_{1/2}$ is the midpoint of activation, z is the maximum slope, F is Faraday's constant, R is the gas constant and T is temperature in Kelvin. The upper and lower asymptotes, A1 and A2, were left to vary, allowing data to be fit in cases where channels were not fully activated in the voltage ranges that can be used with oocytes (Gage and Kobertz, 2004). The isochronal free energy of channel opening, $\Delta G_{iso,}$ was calculated for WT and each mutant Q1/E1 complex using the equation $\Delta G_{iso} = zFV_{1/2}$. For each mutant, $\Delta\Delta G_{iso}$ was calculated as $\Delta G_{iso}^{\ mutant} - \Delta G_{iso}^{\ WT}$. The deactivation time constant (τ_d) was measured by fitting the current at – 80 mV following a 40 mV depolarization to a single exponential.

Periodicity Analysis: The periodicity of $\Delta\Delta G_{iso}$ was determined as previously reported by Swartz et al. using the following equation (Li-Smerin et al., 2000a):

$$P(\omega) = \left(\sum_{j=1}^{n} \left[\left(Vj - \langle V \rangle \right) \sin(j\omega) \right] \right)^2 + \left(\sum_{j=1}^{n} \left[\left(Vj - \langle V \rangle \right) \cos(j\omega) \right] \right)^2$$

$P(\omega)$ is the power spectrum as a function of angular frequency, ω, and was determined for E1 C-terminal segments of 7 to 10 residues where ‹V› is the average $|\Delta\Delta G_{iso}|$ for each segment, V_j is the $\Delta\Delta G_{iso}$ at position j, and n is the number of residues in a segment. Since α-helices are defined as having 3.6 residues per turn, a peak angle at 100° indicates an ideal α-helix. Transmembrane helices have shown peak angles shifted to higher frequencies, and since this membrane-abutting C-terminal region is presumably an extension of the membrane-spanning helix, this analysis was centered at 105° (Rees et al., 1989; Li-Smerin et al., 2000a). The α-periodicity index (α-PI) is the average value of $P(\omega)$ in this helical range (90° – 120°) relative to the average value of $P(\omega)$ over the entire power spectrum and is a quantitative assessment of helical character:

$$\alpha\text{ - PI} = \left[1/30 \int_{90^\circ}^{120^\circ} P(\omega) d\omega \right] / \left[1/180 \int_{0^\circ}^{180^\circ} P(\omega) d\omega \right];$$

values for α-PI > 2 are considered indicative of an α-helix. For mathematical analyses that necessitated the inclusion of the nonfunctional D76A mutant, a $\Delta\Delta G_{iso}$ value of 1 kcal/mol was used to maintain the α-PI and peak angle calculated for the K69-N75 segment.

Cell Surface Luminometry: The surface expression of HA-tagged E1 proteins was measured by luminometry (Zerangue et al., 1999). Oocytes were injected with 7.5 ng Q1 and 3.75 ng WT or mutant E1-HA. After 3-5 days, currents were recorded from a few oocytes expressing WT E1-HA complexes to ensure that functioning complexes were present at the cell surface. ND96B containing 1% BSA was used to block and wash oocytes, as well as dilute antibodies. Oocytes were cooled to 4°C, blocked for 30 min, and primary antibody (1 μg/mL rat monoclonal α-HA; Roche) was applied for 1 h at 4°C. Oocytes were washed (8 × 5 min), incubated for 40 min with secondary antibody (2 μg/mL α-rat $F(ab)_2$; Jackson ImmunoResearch Laboratories), and washed again (5 × 10 min). Oocytes were finally washed with ND96B containing no BSA for 1 h at 4°C, individually placed in wells with 50 μL of ND96B solution and mixed with 50 μL of the SuperSignal ELISA Femto Maximum Sensitivity Substrate (Pierce Chemical Co.). The signal at 405 nm was integrated for 10 s after a 20 s delay using a Veritas Microplate luminometer (Turner Biosystems). Data is reported in relative light units (RLU).

Results

The C-terminal sequence that abuts the predicted transmembrane domain of E1 is required for Q1 modulation (Tapper and George, 2000), suggesting that a protein-protein interaction exists between Q1 and E1 in this region. To identify the C-terminal residues in E1 that face the Q1 channel complex and to determine whether this region possesses any secondary structure, E1 residues 68-86 were individually mutated to alanine, expressed with Q1 channels in *Xenopus* oocytes, and the changes in gating were measured using two-electrode voltage clamp (TEVC). For native alanine residues, leucine was used to induce a perturbation; for native serine residues, both alanine and leucine mutants were examined.

Of the 19 E1 C-terminal residues examined, only one mutant, D76A, did not express current. This was expected given that the long QT mutation (D76N) and the equivalent mutation in rat affords a non-functional Q1 channel complex (Wang and Goldstein, 1995; Splawski et al., 1997; Bianchi et al., 1999). Currents elicited from voltage depolarizations of wild type (WT) and representative mutant Q1/E1 complexes in high external K^+ are shown in Figure 2-1A. To compare the voltage-gating of the WT and mutant Q1/E1 complexes, activation curves were generated by measuring the tail current after repolarization and plotting normalized current versus depolarization potential (Figure 2-1B). Standard tail-current analysis requires that channels reach equilibrium between the open and closed states before repolarization; however, Q1/E1 complexes do not reach equilibrium even after 90-second depolarizations (Takumi et al., 1988).

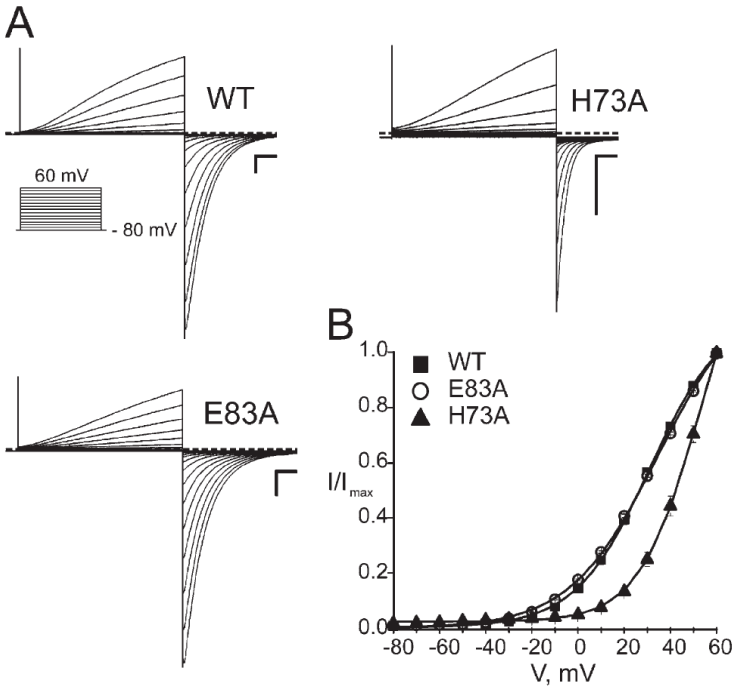

Figure 2-1 E1 alanine mutants show diverse gating properties

(A) Two-electrode voltage clamp recordings of WT, H73A, and E83A mutant channels expressed in *Xenopus* oocytes. Currents were recorded in KD98 solution. Dashed line indicates zero current. Scale bars represent 1 μA (y-axis) and 0.5 s (x-axis). Inset, protocol of 4 s depolarizations from −80 to 60 mV at 10-mV increments used to elicit currents shown.

(B) Voltage activation curves for WT and representative mutant channel complexes calculated from tail current analysis. Solid curves represent Boltzmann fits to the data. Data was averaged from 5-10 oocytes each ± SEM and is presented in Table 2-1.

Therefore, tail current amplitudes following 4 s pulses allowed an isochronal measure of Q1/E1 voltage dependence. Activation curves were fit to a Boltzmann equation, and from the Boltzmann fit, the voltage of half maximal activation ($V_{1/2}$) and slope factor (z) were determined for WT and each mutant Q1/E1 complex (Table 2-1). These parameters were used to calculate the isochronal free energy of Q1/E1 complex opening at zero voltage (ΔG_{iso}), and for each mutant, $\Delta\Delta G_{iso}$ was also determined ($\Delta G_{iso}^{mutant} - \Delta G_{iso}^{WT}$). As in previous perturbation studies (Monks et al., 1999; Hong and Miller, 2000; Li-Smerin et al., 2000a; Li-Smerin et al., 2000b), residues with a $|\Delta\Delta G_{iso}| > 1$ kcal/mol were defined as high impact. Using this arbitrarily defined cut-off, nine mutants scored as high impact, all of which resulted in stabilization of the closed state and acceleration of the deactivation kinetics when compared to WT. For the native serine residues, where alanine and leucine substitutions were individually examined, both S68A and S68L were defined as high impact, only S74L scored as high impact, and both S84 mutants were low impact.

To determine whether there was a periodicity of high and low impact mutants, the C-terminal residues were plotted on a helical wheel (Figure 2-2, center). An α-helical pattern was not immediately apparent by simple visual inspection, nor by Fourier periodicity analysis (*vide infra*). While plotting the data on a helical wheel diagram, a helical pattern was initially observed for the bottom half of the region, but the pattern disappeared conspicuously after a proline residue. Proline disruption of helical segments has been previously detected in transmembrane segments of two voltage-gated K^+ channels by perturbation mutagenesis (Hong and Miller, 2000; Li-Smerin et al., 2000a).

Table 2-1. Electrophysiological Properties of KCNE1 Mutants[1]					
Construct	$V_{½}$ (mV)	*z*	ΔG	ΔΔG	$\tau_{deactivation}$ (ms)
E1	31.3 ± 1.1	1.56 ± 0.03	1.02 ± 0.05	--	665 ± 80
S68A	60.0 ± 1.2	2.20 ± 0.06	3.04 ± 0.09	2.02 ± 0.10	131 ± 5
S68L	51.8 ± 1.6	1.90 ± 0.13	2.26 ± 0.15	1.24 ± 0.16	139 ± 7
S68D	43.6 ± 1.0	1.90 ± 0.07	1.91 ± 0.08	0.89 ± 0.09	156 ± 6
S68E	44.8 ± 1.0	2.05 ± 0.12	2.11 ± 0.09	1.09 ± 0.10	145 ±14
K69A	28.1 ± 1.6	1.84 ± 0.03	1.19 ± 0.06	0.17 ± 0.08	350 ± 28
K70A	56.1 ± 0.6	2.24 ± 0.06	2.90 ± 0.09	1.88 ± 0.10	105 ± 4
K70Q	54.5 ± 0.8	2.04 ± 0.08	2.27 ± 0.08	1.25 ± 0.09	132 ± 3
L71A	42.6 ± 2.6	2.04 ± 0.08	2.02 ± 0.18	1.00 ± 0.19	256 ± 16
E72A	43.0 ± 0.8	1.90 ± 0.02	1.88 ± 0.03	0.86 ± 0.06	362 ± 18
H73A	52.3 ± 3.2	2.03 ± 0.02	2.40 ± 0.10	1.38 ± 0.11	176 ± 3
S74A	34.1 ± 0.9	1.61 ± 0.03	1.27 ± 0.04	0.25 ± 0.06	496 ± 32
S74L	53.4 ± 1.5	1.94 ± 0.09	2.37 ± 0.09	1.35 ± 0.10	200 ± 12
S74I	44.4 ± 1.4	2.17 ± 0.03	2.22 ± 0.08	1.20 ± 0.09	189 ± 10
S74M	30.3 ± 2.1	1.90 ± 0.03	1.35 ± 0.11	0.33 ± 0.12	255 ± 22
N75A	27.9 ± 1.5	1.65 ± 0.02	1.06 ± 0.06	0.04 ± 0.08	644 ± 42
D76A	NF	NF	NF	NF	NF
P77G	ND	ND	ND	ND	ND
P77A	38.4 ± 2.7	1.65 ± 0.05	1.41 ± 0.08	0.39 ± 0.09	406 ± 9
P77L	39.5 ± 1.7	1.52 ± 0.08	1.38 ± 0.04	0.36 ± 0.06	381 ± 19
F78A	69.5 ± 6.4	1.50 ± 0.10	2.14 ± 0.12	1.12 ± 0.13	161 ± 14
N79A	45.6 ± 0.9	2.12 ± 0.04	1.98 ± 0.07	0.96 ± 0.09	179 ± 4
V80A	43.7 ± 1.3	1.55 ± 0.02	1.39 ± 0.04	0.37 ± 0.06	258 ± 13
Y81A	74.7 ± 1.0	1.85 ± 0.02	2.88 ± 0.15	1.86 ± 0.16	112 ± 3

Construct	$V_{½}$ (mV)	*z*	ΔG	ΔΔG	$\tau_{deactivation}$ (ms)
I82A	59.4 ± 1.2	2.20 ± 0.03	2.67 ± 0.04	1.65 ± 0.06	145 ± 5
E83A	34.6 ± 0.8	1.34 ± 0.02	1.06 ± 0.02	0.04 ± 0.05	630 ± 50
S84A	44.6 ± 1.2	1.90 ± 0.06	1.95 ± 0.05	0.93 ± 0.05	317 ± 16
S84L	37.5 ± 4.2	1.13 ± 0.03	0.97 ± 0.09	-0.05 ± 0.10	449 ± 52
D85A	48.0 ± 2.5	1.98 ± 0.04	2.18 ± 0.13	1.16 ± 0.14	297 ± 20
A86L	24.8 ± 0.8	1.61 ± 0.03	0.92 ± 0.03	-0.10 ± 0.06	874 ± 57

[1]Data from individual activation curves and deactivation time constants in KD98, obtained from 4–12 oocytes. Activation curves were fit to a Boltzmann function as described in Materials and Methods. $V_{½}$ is the voltage of half-maximal activation and *z* is the slope factor. Time constants of deactivation were fit to a single exponential as described in the Materials and Methods. Values are mean ± SEM of several independent measurements. NF, non-functional mutant, ND, no current detected.

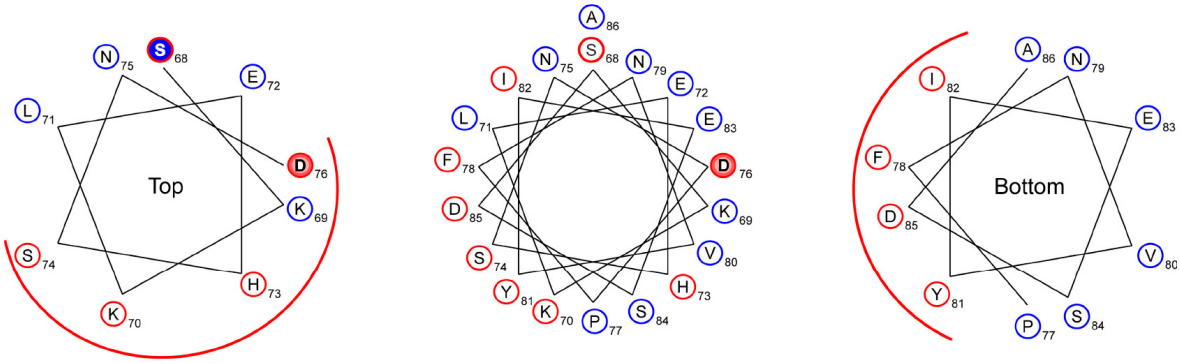

Figure 2-2 Periodicity of gating perturbations in the E1 C-terminal domain

Center, helical wheel diagram of the 19 C-terminal E1 residues examined. Red circles indicate residues with $\Delta\Delta G_{iso} > 1$ kcal/mol, blue circles indicate $\Delta\Delta G_{iso} \leq 1$ kcal/mol.

Power spectrum analysis indicates a peak angle of 125° and a-PI for of 1.77 for the entire C-terminal segment. When residues above and below Proline 77 are plotted on separate helical wheels (**left** and **right**), high impact residues (red) and low impact residues (blue) segregate to separate faces of each helical diagram. Each high impact face is denoted by a red line. S68A is a high impact residue on the low impact face (filled blue with red outline). D76A is expressed at the plasma membrane but is a nonfunctional mutant, as determined by cell surface luminometry (red fill).

Therefore, amino acids above and below the proline were plotted on two separate helical diagrams. The residues on the bottom helical wheel (Figure 2-2, right) segregated on two distinct faces. Clustering of the high and low impact residues was also observed for the top helical diagram (Figure 2-2, left); however, there were two high impact serines (S68 and S74) and the non-functional mutant (D76A) that warranted further experimental investigation.

S68A is a noticeable outlier in the top helical wheel, landing on the low impact face. Sequence analysis indicates that S68 is within a putative protein kinase C (PKC) consensus sequence, suggesting that this serine may be phosphorylated. Since the premise of perturbation mutagenesis is that alterations in side chain volume lead to disruption of protein-protein interactions and thus channel function, it is possible that S68A scored as high impact due to the inability to posttranslationally place a negative charge at this position, and not due to a change in side chain volume. To test this hypothesis, S68 was mutated to aspartic and glutamic acid: two commonly used imperfect isosteres of phoshorylated serine. Figure 2-3 A shows the current-voltage relationships of the S68A, D, and E mutants. Activation curves (Figure 2-3 B) show that substitution with either aspartic or glutamic acid had less of an effect ($\Delta\Delta G_{iso} \sim 1$ kcal/mol) than the alanine mutant ($\Delta\Delta G_{iso} \sim 2$ kcal/mol). If S68 is phosphorylated by PKC, mutation of the surrounding consensus sequence should also have a similar effect on Q1/E1 complex function. Substituting K70 with glutamine is predicted by oriented peptide libraries to disrupt the PKC consensus sequence (Nishikawa et al., 1997), yet this polar residue produces a nominal change in side chain volume.

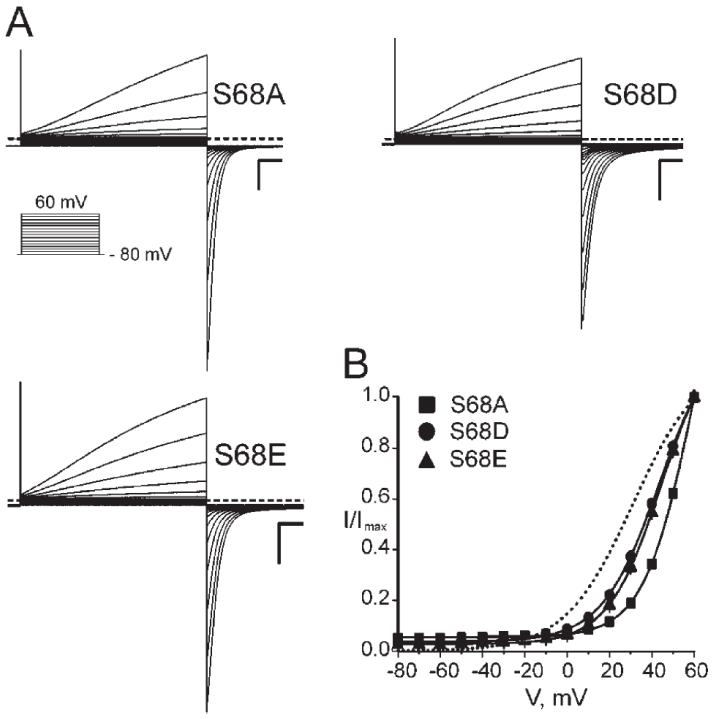

Figure 2-3 Negatively charged side chains produce smaller perturbations than alanine at position S68

(A) TEVC recordings of S68A, S68D, and S68E channels expressed in *Xenopus* oocytes. Currents were recorded in KD98 solution. Dashed line indicates zero current. Scale bars represent 1 μA (y-axis) and 0.5 s (x-axis). Inset, protocol of 4-s depolarizations from −80 to 60 mV at 10-mV increments used to elicit currents shown.

(B) Voltage activation curves for S68A, S68D and S68E mutant channels calculated from tail current analysis. Solid curves represent Boltzmann fits to the data. Dotted line indicates Boltzmann fit of WT activation curve. Data was averaged from 8-10 oocytes each ± SEM.

Like S68A, the K70Q mutant shifts the voltage-dependence of activation of the Q1/E1 complex in favor of the closed state (Table 2-1).

Of the native serines in the E1 C-terminal region, S74 was unique in that the alanine mutant was defined as low impact whereas the leucine mutant was high impact. Upon breaking the region in two halves, S74 was positioned at the high/low impact interface of the helical wheel (Figure 2-2, left). If S74 is situated at the water-protein interface, side chains with a higher degree of rotational freedom could use the adjacent aqueous environment to adopt a conformation that would maintain productive protein-protein interactions without steric clashes, whereas more rigid, branched side-chains could not. Conveniently, leucine, isoleucine, and methionine have approximately the same Van der Waals volume (Creighton, 1992), yet their flexibility and the three-dimensional space that they occupy is significantly different. Figure 2-4 shows that mutating E1 S74 to the straight-chain methionine afforded a Q1-complex similar to WT, whereas mutation to the β-branched isoleucine resulted in a Q1/E1 complex similar to leucine, which was defined as high impact (Table 2-1).

D76A was the only alanine mutation that did not express measurable current when co-injected with Q1 mRNA. There are two possibilities to explain the negligible current observed with this mutation: (1) the Q1/D76A complex is non-functional; or (2) the Q1/D76A complex cannot reach the plasma membrane. To discern between these two, whole oocyte cell surface luminometry was employed to determine whether an extracellularly HA-tagged D76A could reach the plasma membrane.

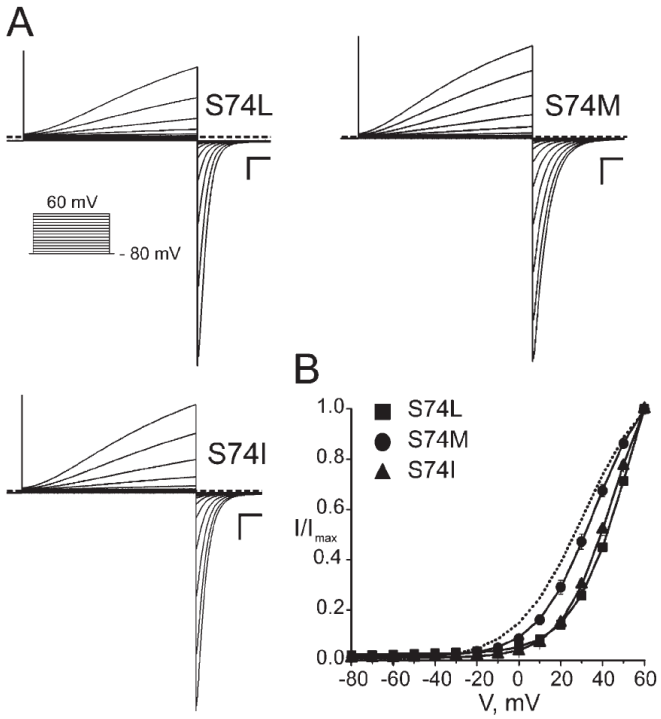

Figure 2-4 Branched amino acids cause larger perturbations at position S74

(A) TEVC recordings of S74L, S74M, and S74I channels expressed in *Xenopus* oocytes. Currents were recorded in KD98 solution. Dashed line indicates zero current. Scale bars represent 1 μA (y-axis) and 0.5 s (x-axis). Inset, protocol of 4-s depolarizations from −80 to 60 mV at 10-mV increments used to elicit currents shown.

(B) Voltage activation curves for S74 mutant channels calculated from tail current analysis. Solid curves represent Boltzmann fits to the data. Dotted line indicates Boltzmann fit of WT activation curve. Data was averaged from 6-10 oocytes each ± SEM.

Figure 2-5 shows that D76A protein is present at the plasma membrane similarly to WT and the long QT causing mutant D76N, which is non-functional at the cell surface (Wang and Goldstein, 1995; Gage and Kobertz, 2004). Since the Q1/D76A complex is at the plasma membrane but not conducting, this mutant was scored as a high impact residue.

Splitting the E1 C-terminal region into two domains was based on the observation that the periodicity of high and low impact mutants shifted at P77, suggesting a kink or turn at this position. To experimentally test whether the presence of a helix-breaking residue at this position was required for proper Q1/E1 complex function, P77 was replaced with amino acids that are known to either induce flexibility or maintain α-helicity. Both alanine and leucine are often found in helical regions and are considered helix-inducing (Rohl et al., 1996). Substitution of either of these residues at position 77 produced Q1-complexes similar to WT (Table 2-1). Exchanging the proline for the highly flexible glycine residue did not afford currents above uninjected controls.

The lack of an obvious trend with this mutagenic discourse prompted the use of Fourier transform periodicity analysis to determine the degree of helicity in each segment and the location of the helical phase change. This non-biased analysis has been used to define the helical segments within an entire voltage-sensing domain of a mammalian K^+ channel (Li-Smerin et al., 2000a). Determining the periodicity of a region using a power spectrum requires a $\Delta\Delta G_{iso}$ value for every residue. To satisfy this requirement, this analysis excluded both D76A, since it was non functional, and S68A, given the uncertainty of the native state of this side chain in the functioning Q1/E1 complex.

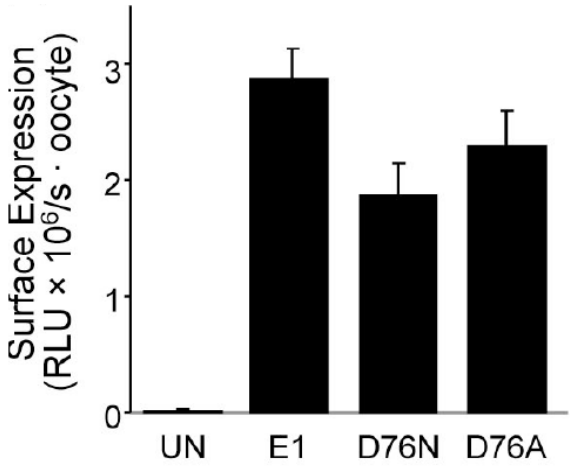

Figure 2-5 D76A is expressed at the cell surface

Whole oocytes luminometry was used to quantify the surface expression of HA-tagged E1 peptides (E1, D76N, D76A) and uninjected controls (UN). Luminescence is reported in relative light units (RLU). Error bars represent SEM from 10-20 oocytes.

Figure 2-6 shows the power spectra for K69 – N75 and P77 – A86 when the E1 C-terminal region is broken into two halves at P77. Both spectra show a peak angle within the boundaries of helicity (90˚ – 120˚) and with α-periodicity index (α-PI) > 2. These results are highly indicative of two helical domains, as was observed using simple helical wheel models (Figure 2-2). To determine whether P77 was the ideal location to divide the E1 C-terminal domain, the breakpoint position was varied. Since a $\Delta\Delta G_{iso}$ value cannot be assigned for D76A, a placeholder value was used for D76 to maintain the helical trajectory of the K69 – N75 segment. Propagation of the domain to include P77 and F78 resulted in sharp drop in α-PI, indicating that residues past D76 should not be included in the top segment (Table 2-2). For the bottom segment, the α-PI increased as the analysis was extended to include the proline while the peak angle remained consistent for a helix.

However, inclusion of D76 using any high impact value greater than 1 kcal/mol decreased the α-PI, indicating that this high impact residue was out of helical phase with the bottom segment. Taken together, dividing the entire E1 C-terminal domain at any position other than P77 resulted in less helical character for either the top or the bottom segments.

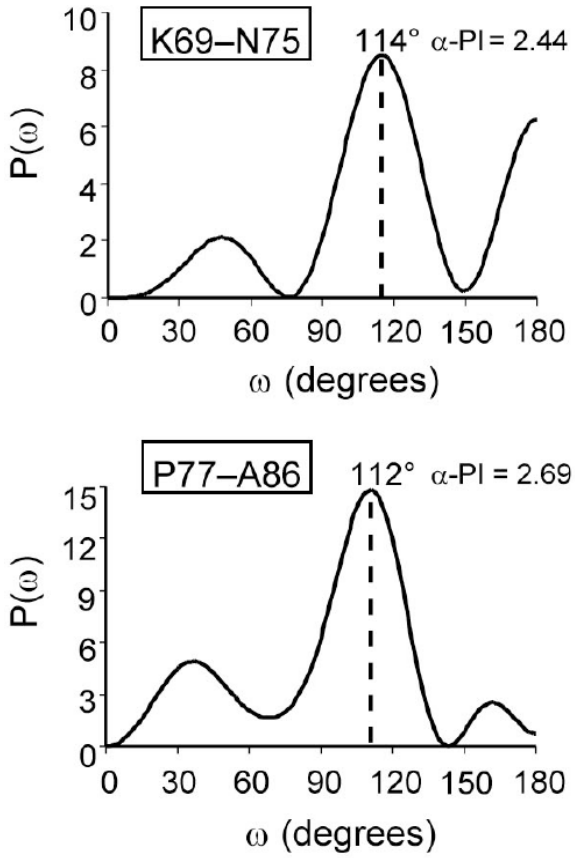

Figure 2-6 Periodicity analysis of the top and bottom segments of the E1 C-terminal domain

P(ω) is plotted as a function of angular frequency (ω) to generate a power spectrum of the $\Delta\Delta G_{iso}$ values for each segment. A value of 1 kcal/mol was assigned for the non-functional D76A mutant. The primary peak occurs at 114° for the top segment and 112° for the bottom.

Table 2-2. α-helical characteristics of C-terminal E1 segments[1]

Segment	α-PI	Peak angle	Segment	α-PI	Peak angle
K69 – N75	2.44	114°	P77 – A86	2.69	112°
K69 – P77	1.61	123°	F78 – A86	2.53	109°
K69 – F78	1.51	126°	N79 – A86	2.20	111°

[1]Data from power spectrum periodicity analysis of $\Delta\Delta G_{iso}$ for residues in each segment. Power spectra, α-PI and peak angle values were calculated as described in Materials and Methods. For the top segments that contain D76, a placeholder value of 1 kcal/mol was used, which maintains the helical trajectory of the K69 – N75 segment.

Discussion

This chapter applied perturbation mutagenesis and helicity analysis to identify secondary structural elements in the conserved cytoplasmic region of the E1 β-subunit. Previous perturbation studies have primarily relied on comparing the free energy of channel opening of mutant channels versus wild type (Monks et al., 1999; Hong and Miller, 2000; Li-Smerin et al., 2000a; Li-Smerin et al., 2000b). Measuring isochronal ΔΔG values permitted use of this parameter for Q1/E1 complexes, which do not reach equilibrium under standard-length test depolarizations. Although these values are not free energies, they allowed for a comparative analysis of the effect of mutations in E1 on Q1 function. Half of the mutations studied in the E1 C-terminus produced $| \Delta\Delta G_{iso} | > 1$ kcal/mol—an arbitrarily defined cut-off for a high impact residue, but an empirically supported definition (Monks et al., 1999; Hong and Miller, 2000; Li-Smerin et al., 2000a; Li-Smerin et al., 2000b). Changes in deactivation kinetics have also been used to define high impact residues, though a specific cut-off value has not emerged from previous reports (Monks et al., 1999; Hong and Miller, 2000). Graphing the deactivation kinetics of the E1 mutants reveals that a 3-fold acceleration of channel closing rate mirrors the trend observed with isochronally measured $\Delta\Delta G_{iso}$ (Figure 2-7). Only one mutant, D76A, was refractory from this straightforward functional analysis since it did not generate measurable currents. However, cell surface labeling experiments show that this mutant is at the plasma membrane and is non-functional, and thus is defined as high impact.

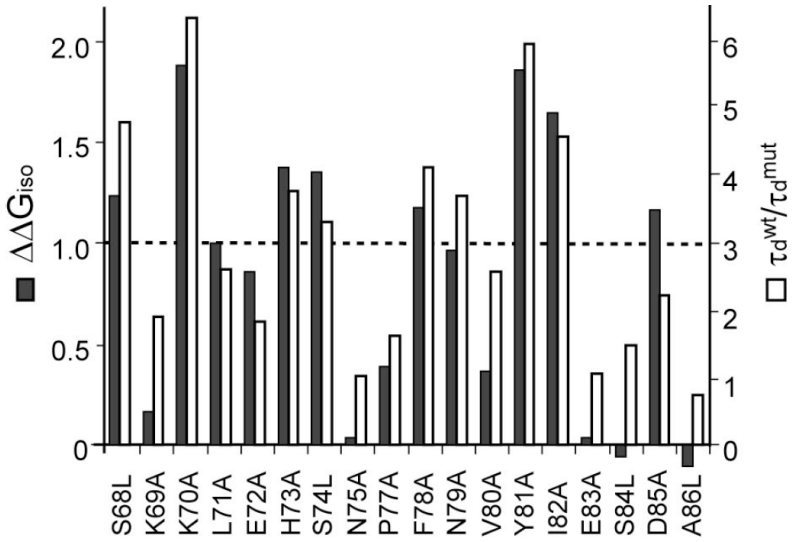

Figure 2-7 Changes in deactivation rate mirror $\Delta\Delta G_{iso}$ measurements

Double bar graph comparing ΔΔGiso and deactivation rate (τ_d) for the E1 C-terminal alanine and leucine mutants. Solid bars indicate $\Delta\Delta G_{iso}$, open bars $\tau_d^{WT}/\tau_d^{mutant}$. The dashed line denotes the cutoff values for $\Delta\Delta G_{iso}$ and $\tau_d^{WT}/\tau_d^{mutant}$. Values for $\tau_d^{WT}/\tau_d^{mutant}$ > 1 indicate accelerated deactivation kinetics.

Although only two mutations (D76A and the Long QT-causing D76N) have been examined at this position, it is interesting that both substitutions result in non-functional complexes that efficiently traffic to the plasma membrane.

Plotting the residues on helical wheels resulted in no obvious clustering of high impact residues (Figure 2-2, center). Periodicity analysis using a power spectrum confirmed that no helical pattern was present: both the peak angle (125˚) and α-PI (1.77) were inconsistent with the region being a continuous helix. However, breaking the cytoplasmic region into two domains at a conserved proline (P77) segregated the high and low impact residues to distinct faces on helical wheels. In addition, Fourier periodicity analysis indicates that both domains have significant helical character (Table 2-2), which supports the arbitrarily defined 1 kcal/mol cut-off value used for the helical wheel diagrams (Figure 2-2). Moreover, this depiction places all known long QT mutants in this region on the high impact face. Given that mutants on the high impact face markedly shift the gating of Q1/E1 complexes, this analysis predicts that these residues directly interact with the channel complex. This prediction is supported in high resolution detail with the crystal structures of voltage-gated K^+ channels (Jiang et al., 2003a; Jiang et al., 2003b; Long et al., 2005a), which verified that the high impact faces identified by previous perturbation studies are involved in protein-protein interactions within the voltage-sensing domain.

Although a convincing pattern was observed with helical wheel diagrams for the E1 C-terminal domain, S68A did not segregate to the high impact face, even though it had the highest $\Delta\Delta G_{iso}$ calculated. S68 is within a putative PKC consensus sequence.

Disruption of the PKC site by mutation of the critical +2 basic residue (K70) to either glutamine or alanine resulted in Q1/E1 complexes with right-shifted activation curves similar to S68A, which cannot be phosphorylated. Although phosphorylation of E1 at this serine has not been observed experimentally, it has been detected in the homologous serine in E3 (Abbott et al., 2006). Substitution of S68 to either aspartic or glutamic acid, to mimic phosphoserine, showed that the more voluminous, but negatively charged side chains had less of an effect on Q1/E1 gating than the removal of hydroxyl group by alanine mutagenesis. These preliminary data suggest that E1 may be phosphorylated at S68, but requires further biochemical support and verification in native tissues.

Unlike S68 and S84, S74 was uniquely sensitive to changes in amino acid side chain volume in that only the bulkier S74L mutant scored as high impact. Helical analysis revealed that this residue was at the edge of the high impact face, prompting further experimental examination. Isovoluminous substitution showed that branched amino acids (isoleucine, leucine) were less tolerated than the straight chain methionine side chain, which scored as a low impact residue using both criteria ($\Delta\Delta G_{iso}$ and τ_d). These results are consistent with the notion that S74 lies at the water-protein boundary since the flexible methionine side chain can adopt a productive protein-protein interaction between E1 and the Q1-channel complex while utilizing the adjacent aqueous environment without energetic penalty.

Previous perturbation studies of voltage-gated K^+ channels identified a proline residue in the S3 helix that disrupted the helical pattern of this transmembrane domain (Hong and Miller, 2000; Li-Smerin et al., 2000a). The ensuing proposal that S3 is kinked

at this proline residue was confirmed by three high resolution crystal structures of voltage sensing domains (Jiang et al., 2003a; Jiang et al., 2003b; Long et al., 2005a). Since the perturbation results presented in this chapter describe a strong helical pattern when the E1 C-terminal domain is divided in half at a proline residue, P77 probably induces a kink or turn at this position. Attempts to mimic this kink by replacing P77 with the helix breaking residue, glycine, were hindered since the Q1/P77G complex produced background-level current. To determine if the proline geometry was required for proper modulation of Q1 channels, P77 was replaced with alanine and leucine, two residues that have a high helix propensity (Rohl et al., 1996). When these mutants were expressed with Q1 subunits, K^+ currents and gating characteristics similar to wild type Q1/E1 complexes were observed. Identical results (with alanine and tryptophan) were also obtained for the helix-kinking proline in the S3 segment of K^+ channel voltage sensors (Hong and Miller, 2000; Li-Smerin et al., 2000a), suggesting that detection of proline kinks using channel function and simple site-directed mutagenesis may not be possible. This conclusion is further supported by a systematic investigation of conserved proline residues in membrane proteins, which has shown that many protein-protein interfaces evolve ancillary interactions to stabilize kinked helices thus obviating the need for proline residues to maintain the bent geometry (Yohannan et al., 2004).

Since mutagenesis could not elucidate whether a turn or kink was present at P77, power spectrum analysis aided in identifying the location of the phase change in the E1 C-terminal domain. Using this mathematical approach, breaking the domain at P77 resulted in two segments with the greatest α-PI and peak angles most consistent with

helices that are adjacent to a transmembrane domain (Table 2-2). This analysis indicates that the E1 C-terminal domain is helical with either a kink at P77 (Figure 2-8) or the domain experiences a different protein environment above the proline residue, which may also be influenced by PKC phosphorylation. Sequence similarity of this membrane-abutting domain predicts that E2, E3, and E5 will possess a similar structural motif and protein environment when co-assembled with Q1 subunits.

This conserved structural scaffold adds to the growing body of evidence that the E1 C-terminal domain is critical for Q1 channel modulation. Initial E1 deletion studies showed that removal of the membrane-abutting cytoplasmic domain eliminates the hallmark slow activation and deactivation kinetics of the Q1/E1 complex (Tapper and George, 2000). An E3 deletion study concluded that while the E1 C-terminus is required for Q1 modulation, the homologous region in E3 is not necessary (Gage and Kobertz, 2004). The alanine mutants described in this chapter also support the 'bipartite model' of Q1 modulation by KCNE peptides. Alanine mutants in E1 had significant effects on the voltage-dependence and deactivation kinetics of Q1/E1 complexes whereas the equivalent mutations in E3 are predicted to have no measurable effect on the constitutively conducting Q1/E3 complex. Furthermore, tryptophan mutants in the E1 transmembrane domain—though structurally informative—were consistently less perturbative on Q1/E1 complex function than C-terminal E1 alanine mutants (Chen and Goldstein, 2007).

The cytoplasmic E1 C-terminal domain also provides a structural platform for potential interactions with tethered water soluble regulatory proteins.

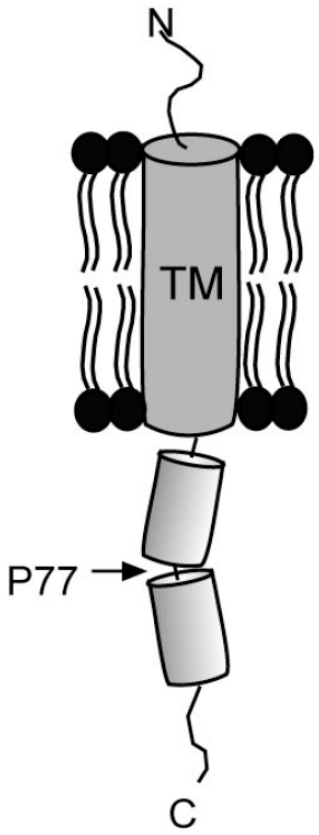

Figure 2-8 The transmembrane-abutting C-terminal domain of E1 contains two helical regions

A cartoon of the Cytoplasmic E1 C-terminal domain split into two helical regions by a kink or turn at P77.

Calmodulin binds the Q1 C-terminus relatively close to the S6 transmembrane segment and facilitates channel assembly and calcium sensitivity (Shamgar et al., 2006). Adjacent to the Q1 calmodulin binding site is a leucine zipper sequence that is required for yotiao, an A-kinase anchoring protein, to bind (Marx et al., 2002). Anchoring of yotiao to the Q1 C-terminus targets cAMP-dependent protein kinase (PKA) and protein phosphatase 1 (PP1), which control the phosphorylation state of the Q1 N-terminus. Moreover, this PKA-mediated modulation can be disrupted by genetic mutations within the E1 cytoplasmic domain (Kurokawa et al., 2003). Thus, the manifold nature of Q1/E1 complex regulation suggests that high impact regions identified in the C-terminus of E1 may be revealing protein-protein interactions not only with Q1 α-subunits, but also with tethered cytoplasmic regulatory proteins.

CHAPTER III: KCNE Peptides Differently Affect Voltage Sensor Equilibrium and Equilibration Rates in KCNQ1 K^+ Channels

Abstract

Q1 voltage-gated K^+ channels assemble with the family of KCNE type I transmembrane peptides to afford membrane-embedded complexes with diverse channel gating properties. Q1/E1 complexes generate the very slowly activating cardiac I_{Ks} current whereas assembly with E3 produces a constitutively conducting complex involved in K^+ recycling in epithelia.

This chapter examines the influence of E1 and E3 on voltage sensing in Q1 channels by monitoring the position of S4 voltage sensors in Q1/KCNE complexes using cysteine accessibility experiments. A panel of Q1 S4 cysteine mutants was expressed in *Xenopus* oocytes, treated with the membrane-impermeant, cysteine-specific reagent 2-(trimethylammonium) ethyl methanethiosulfonate (MTSET), and the voltage-dependent accessibility of each mutant was determined. State-dependent mutants were then employed to examine voltage sensing in Q1/E1 and Q1/E3 complexes. The results demonstrate that E1 does not appreciably affect the rate of S4 equilibration, indicating that slow channel gating is not due to slowly moving voltage sensors. In contrast, E3 shifts voltage sensor equilibrium to favor the active state at hyperpolarizing potentials. In total, these results point to voltage sensing as an additional layer of KCNE modulation of K^+ channels and demonstrate that KCNE peptides differently modulate the voltage sensor in Q1 K^+ channels.

Introduction

Electrical excitability depends on the coordinated openings and closings of voltage-gated cation channels. The voltage sensitivity of these integral membrane proteins is mediated by a voltage sensing domain—a dynamic membrane-embedded domain composed of four transmembrane helices (S1-S4) that moves in response to changes in membrane potential (Long et al., 2005a; Long et al., 2005b). The S4 segment of the voltage sensor possesses a high concentration of positively charged amino acids, which account for most of the charges per channel that move across the membrane's electric field (Aggarwal and MacKinnon, 1996; Seoh et al., 1996). The trajectory and distance traversed by the S4 segment is an ongoing debate; however, all investigations agree that S4 moves between a resting and active state (Jiang et al., 2003b; Chanda et al., 2005; Posson et al., 2005; Ruta et al., 2005; Darman et al., 2006). The shuttling of S4 charges between these two states has been followed in several voltage-gated channels using cysteine accessibility methodologies (Yang and Horn, 1995; Larsson et al., 1996; Yang et al., 1996; Yusaf et al., 1996). These studies show that some residues in S4 are state-dependent: inaccessible to aqueous reagents at rest, but upon membrane depolarization they become exposed to the extracellular milieu and modifiable. For voltage-gated Na^+, K^+ and Ca^{2+} channels, depolarization shifts the equilibrium of the S4 segments to the active state, favoring an open activation gate that permits the rapid flow of ions across the membrane. Conversely, the co-dependent relationship between the S4 segment and activation gate is inversely coupled in hyperpolarized-activated cyclic-nucleotide-gated (HCN) channels: hyperpolarization shifts the sensor to the resting state and opens the activation gate (Mannikko et al., 2002; Vemana

et al., 2004). In both classes of voltage-gated channels, the state of the S4 is tightly coupled to the equilibrium of the activation gate (Yellen, 1998).

Q1 channels are voltage-gated K^+ channels found in both electrically excitable and nonexcitable cells. To meet the potassium flux requirements in this variety of tissues, Q1 channels co-assemble with the family of KCNE type I transmembrane peptides, which substantially alter the voltage sensitivity of the channel (McCrossan and Abbott, 2004). Although currents from homomeric Q1 channels are not observed in native tissues, Q1 is a voltage-dependent delayed rectifier K^+ channel when expressed in standard cell lines and *Xenopus* oocytes (Barhanin et al., 1996; Sanguinetti et al., 1996). Q1 co-assembly with E1 peptides forms a complex that generates the cardiac I_{Ks} current: an incredibly slowly activating current involved in maintaining the rhythmicity of the heartbeat (Barhanin et al., 1996; Sanguinetti et al., 1996). Deactivation kinetics of the Q1/E1 complex are also slowed compared to homotetrameric Q1 channels. In contrast, epithelial Q1/E3 complexes are open at both hyperpolarizing and depolarizing potentials and are weakly voltage-dependent (Schroeder et al., 2000). If Q1/E3 complexes do open and close, the gating kinetics of these transitions are nearly instantaneous. The three other KCNE peptides (E2, E4, E5) also profoundly affect Q1 voltage-gating, converting it into a leak channel, a non-conducting channel, and a severely right-shifted channel respectively (Tinel et al., 2000; Angelo et al., 2002; Grunnet et al., 2002).

Most structure-function studies examining KCNE peptide interactions with Q1 have focused on the pore-forming domain (S5-S6) of the channel (Tai and Goldstein, 1998; Tapper and George, 2001; Melman et al., 2004; Panaghie et al., 2006). However,

unlike most Kv-type channels that possess 5 – 7 net positive charges in S4, Q1 has a net charge of +3. Abbott and colleagues linked KCNE peptides' strong influence on Q1 voltage sensitivity to the channel's charge-poor S4 (Panaghie and Abbott, 2007). Q1 was not modulated by E3 when charges were added to its S4 whereas charge removal from Q4 increases susceptibility to E3's modulatory effects. From this work, they proposed that E3 either uncouples the voltage sensor from the cytoplasmic gate or "locks" the voltage sensor in the active state; however, the position and equilibrium of the voltage sensor was not directly examined.

This chapter experimentally addresses the following question: Do E1 and E3 peptides affect the voltage-dependent equilibrium and equilibration rate of the Q1 voltage sensor? For Q1/E1 complexes, the strikingly slow activation kinetics can arise from increasing the energy barrier for one of the two steps of activation: (1) S4 moving from the resting to active state or (2) activation gate opening (Fig. 3-1A). For the constitutively conducting Q1/E3 complexes, E3 either uncouples voltage sensors from the activation gate or shifts the equilibrium of voltage sensors to significantly reside in the active state at hyperpolarized potentials, as hypothesized by Abbott and co-workers (Panaghie and Abbott, 2007) (Fig. 3-1B).

To directly test these sets of possibilities, the S4 residues that were modified only upon depolarization were identified in unpartnered Q1 channels using cysteine accessibility experiments. These state-dependent residues were then used to examine the position and equilibrium of S4 in Q1/E1 and Q1/E3 complexes. The state-dependent S4 residues in Q1/E1 complexes were modified essentially independent of pulse duration,

suggesting that E1 does not affect the time it takes for the voltage sensors to reach equilibrium. In contrast, all modifiable S4 residues in Q1/E3 complexes were rapidly modified irrespective of membrane voltage, indicating that the voltage sensor frequently resides in the active state when E3 is present. These diametrically opposed effects demonstrate the manifold nature of KCNE modulation of Q1 channels.

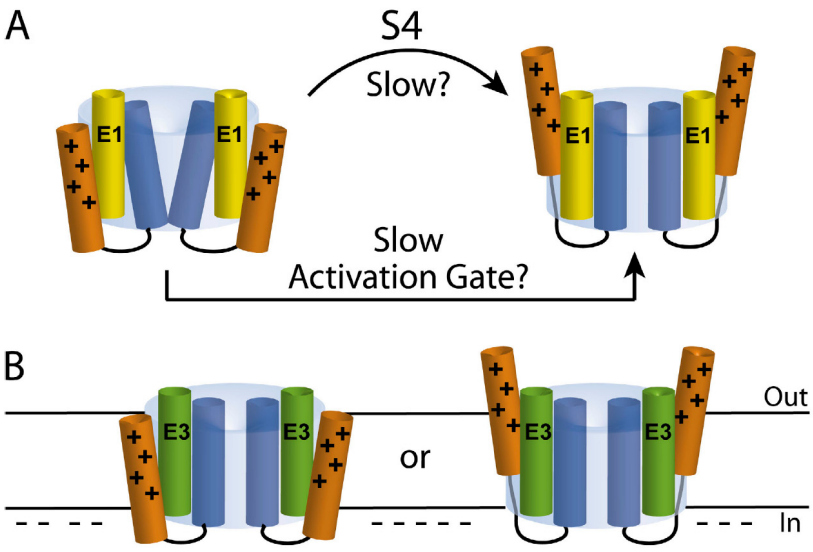

Figure 3-1 Cartoon models depicting possible mechanisms for Q1 channel modulation by E1 and E3

(A) In Q1/E1 channel complexes, slow gating arises from either the slow transition of S4 voltage-sensing domains (orange with positive charges) from resting to active positions, or from slow activation gate opening.

(B) Q1/E3 complexes are open at hyperpolarizing potentials (denoted by negative charges along the cytoplasmic membrane) because S4 voltage sensors are uncoupled from the opening of the gate (left), or because the equilibrium of voltage sensors is shifted to favor the activated state (right).

Materials and Methods

Mutagenesis and in vitro transcription: Human Q1, E1, and E3 were subcloned into vectors containing the 5' and 3' UTRs from the *Xenopus* β-globin gene for optimal protein expression. Single cysteine point mutations were introduced into Q1 using cassette mutagenesis and confirmed by DNA sequencing of the mutated insert. The cDNA plasmids were linearized by MluI digestion, and cRNA was synthesized by run-off transcription using SP6 or T7 RNA polymerase (Promega).

Electrophysiology: Oocytes were surgically removed from *Xenopus laevis* and defolliculated using 2 mg/mL collagenase (Worthington Biochemical Corp.) in OR2 containing (mM): 82.5 NaCl, 2.5 KCl, 1 $MgCl_2$, 5 HEPES, pH 7.4 for 75-90 min. Isolated oocytes were rinsed with and stored in ND96 bathing solution (ND96B) containing (mM): 96 NaCl, 2 KCl, 1.8 $CaCl_2$, 1 $MgCl_2$, 5 HEPES, 50 μg/mL of both gentamicin and tetracycline (Sigma-Aldrich), pH 7.4 at 18°C. Approximately 24 h after extraction, oocytes were microinjected with 27.6 nL total volume of cRNA containing wild type or mutant Q1 (7.5 ng/oocyte), with or without E1 or E3 (3.75 ng/oocyte). After 3–6 days, currents were recorded using Warner Instrument (OC-725) two-electrode voltage clamp (TEVC) and the data were acquired with Digidata 1322A using pClamp 9 (Axon Instruments). Electrodes were filled with 3 M KCl, 5 mM EGTA, 10 mM HEPES, pH 7.6, and had resistance between 0.2 and 1.0 MΩ. Current-voltage relationships were measured in ND96 (in mM): 96 NaCl, 2 KCl, 0.3 $CaCl_2$, 1 $MgCl_2$, 5

HEPES, pH 7.4 by holding at – 80 mV and pulsing for 4 s to potentials between –100 and + 40 mV in 20-mV increments.

MTS modification experiments: To assess extracellular exposure of introduced cysteines, accessibility to the positively charged membrane-impermeant [2-(trimethylammonium)ethyl] methanethiosulfonate (MTSET) or the negatively charged (2-sulfonatoethyl)methanethiosulfonate (MTSES, Toronto Research Chemicals) was determined by measuring changes in current amplitude at + 40 mV.

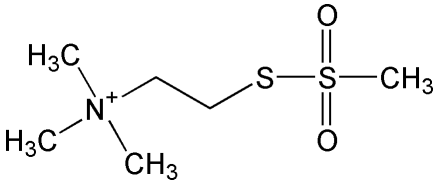

MTSET

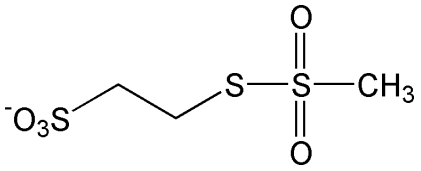

MTSES

Since the half-life of these MTS reagents is ~15 minutes in aqueous solutions (Stauffer and Karlin, 1994), a 0.5 M stock solution was dissolved in water, and aliquots snap frozen in liquid nitrogen. Aliquots were freshly diluted to 0.4 – 1.6 mM in ND96 recording solution immediately prior to perfusion, and every 5 minutes thereafter to maintain a relatively constant concentration for the duration of each experiment.

Two different pulse protocols were used to determine if cysteine exposure was state-dependent. In the open protocol, the membrane was depolarized 11% of the time, for 2 s every 18 s or for 4 s every 36 s. In the closed protocol, the membrane was held at – 80 mV for 99.4% of the time, and only depolarized to + 40 mV for 250 ms every 42 s

or for 500 ms every 84 s. Switching to the open protocol after ~500 s allowed a measure of the extent of modification for residues that were modified slowly in the closed protocol. This was done in the presence and absence of MTSET to rule out any change in current associated with variation in pulse duration and interpulse interval.

To compare each mutant, the currents were normalized using two procedures. For mutants that showed a decrease in current upon MTS modification, the data were normalized such that the current before reagent perfusion was equal to one. For mutants that showed an increase in current upon MTS modification, the baseline was defined as zero and the currents were subsequently normalized based on the full extent of modification. The normalized data were plotted versus reaction time for each MTS modification. All data fit well to a single exponential except for A226C, which required a biexponential fit to extract the fast component of modification.

For the varying pulse duration experiments, five different pulse protocols were used. In each protocol, the membrane was depolarized 11% of the total pulse time. MTSET or MTSES modification was monitored as the membrane was held at – 80 mV and depolarized to + 40 mV for 100 ms every 900 ms, 500 ms every 4.5 s, 1 s every 9 s, 2 s every 18 s or 4 s every 36 s. Modification-induced current changes were monitored at the end of the shortest pulse duration used for each set of experiments. For voltage dependence experiments with I230C/E3, oocytes were held at – 80 mV and pulsed for 4 s to either – 100, – 80, – 40, 0 or 40 mV, followed by a – 30 mV tail pulse. Current changes were monitored at the end of the – 30 mV tail for each voltage potential studied.

Results

Identification of state-dependent S4 residues in KCNQ1 K^+ channels

To determine the influence of KCNE peptides on the position and equilibrium of the voltage sensor, residues in the S4 segment of Q1 were examined for accessibility to an externally applied aqueous cysteine-specific modifying reagent, MTSET. Residues 226–232 were individually mutated to cysteine, expressed in *Xenopus* oocytes, and currents were elicited from a series of test depolarizations using two electrode voltage clamp (TEVC). The majority of the cysteine mutants (A226C, I227C, G229C, I230C, F232C) resembled wild-type Q1 (Fig. 3-2); however, charge neutralization of either of the two arginine residues by cysteine mutagenesis resulted in currents with altered gating kinetics (Fig 3-3, before). R228C afforded small currents that slowly activated; R231C was a constitutively conducting channel. The gating kinetics observed for these Q1 cysteine mutants were nearly identical to those observed when the arginines were mutated to alanine (Panaghie and Abbott, 2007).

These cysteine mutants were then screened for changes in current amplitude or gating kinetics when treated with MTSET. Examination of the Q1 mutants after MTSET treatment revealed that the gating kinetics of the modified channels became nearly instantaneous and were open at hyperpolarized potentials (Fig. 3-3, after). To monitor the rate of cysteine modification, a series of test pulses to 40 mV were elicited for each mutant in the presence of 400 μM MTSET.

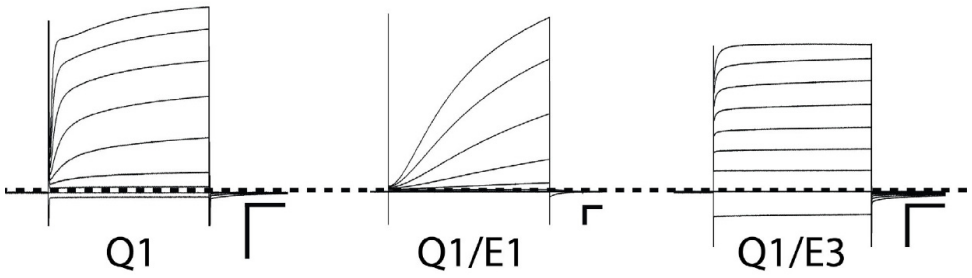

Figure 3-2 TEVC recordings of Q1 channels alone or partnered with E1 or E3 peptides

Oocytes were held at −80mV and currents were elicited from 4-s command voltages from −100 mV to +40 mV in 20-mV increments. Scale bars represent 0.5 μA (y-axis) and 0.5 s (x-axis). Dashed line indicates zero current.

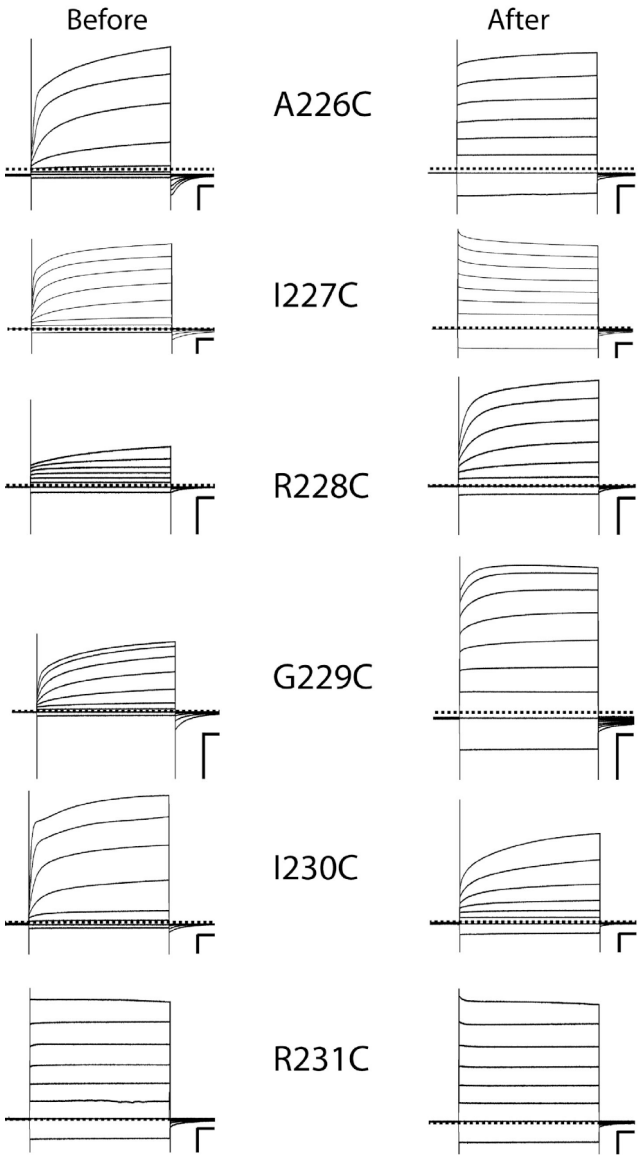

Figure 3-3 S4 cysteine substitutions in Q1 are modified by MTSET.

TEVC recordings of representative Q1 channels with cysteine substitutions in S4 expressed in *Xenopus* oocytes before and after MTSET modification. Oocytes were held at −80 mV, and currents were elicited from 4-s command voltages from −100 mV to +40 mV in 20-mV increments. Scale bars represent 0.5 mA (y-axis) and 0.5 s (x-axis). Dashed line indicates zero current.

Cysteines at positions 226–228 were modified using this protocol as the current increased exponentially with MTSET treatment (Fig. 3-4). Modification-induced current changes were also measurable for G229C and I230C when the MTSET concentration was doubled. R231C and F232C were unaffected by MTSET, indicating that these deeper residues were either not accessible to the reagent, or the modification did not induce a measurable change in current. Since all modifications required MTSET treatment for longer than the half-life of the reagent (~ 15 min) (Stauffer and Karlin, 1994), freshly prepared MTSET was continuously added to the gravity-fed perfusion device every 5 min to maintain a relatively constant concentration (Materials and Methods). Currents from wild-type Q1 expressed alone, with E1, or E3 were unchanged by MTSET (Fig. 3-4), demonstrating that changes in current observed with the mutants were due to the presence of cysteines in the S4 segment.

Once S4 mutants that were measurably modifiable by MTSET were identified, the state dependence of modification was determined. The rate MTSET of modification was compared using two test pulse protocols: open and closed. In the closed protocol, the channels are held at – 80 mV for the majority of the pulse duration and only briefly depolarized to ascertain MTSET modification rate; therefore, the S4 voltage sensors are primarily in the resting state. In the open protocol, the channels are depolarized ~ 18-fold more, which shifts the equilibrium of the S4 voltage sensors to favor the active state. Thus, state-dependent S4 residues are modified faster in the open protocol compared to the closed, whereas state-independent residues are modified at a similar rate independent of the protocol used.

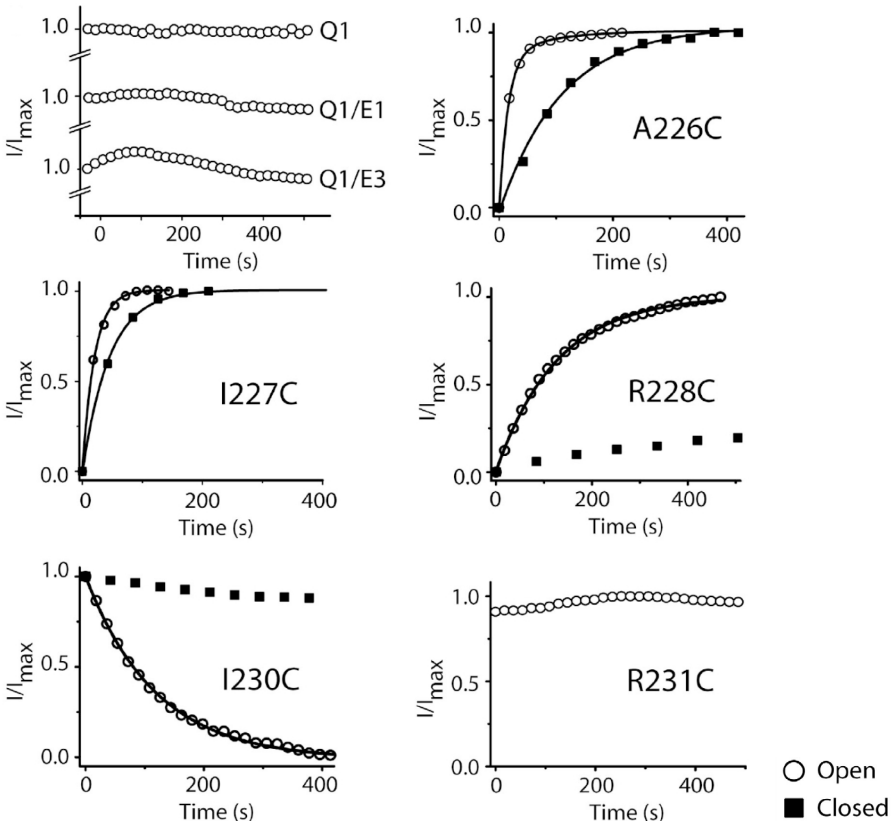

Figure 3-4 S4 cysteine substitutions in Q1 show state-dependent MTSET modification

Change in current monitored over time using 40-mV test pulses with continuous perfusion of MTSET. For negative controls, 800 μM MTSET was used for Q1 and Q1/E3, 1600 μM for Q1/E1. The data were plotted on the same y-axis scale as the cysteine mutants and are separated by line hatches. Open circles represent the 'open' protocol where channels were depolarized for 11% of the total time; filled squares represent the 'closed' protocol with depolarizations of 0.6% of the total time. Currents from the open and closed protocols were measured ~ 5 ms before the end of the shortest depolarizing pulse and were normalized to the maximal change in current for comparison. Curves were fit to single or double exponentials to calculate reaction rate constants. Fitted parameters are presented in Table 3-1.

The rates of S4 cysteine modification in the open and closed protocols are compared in Figures 3-4 and 3-5. Modification rates for the first two residues (A226C, I227C) could be measured in both the open and closed protocols. Since the "open" protocol is only open 11% of the test pulse cycle, MTSET reactions were expected to exhibit biexponential kinetics for the cysteine mutants that were appreciably modified in both states, as long as the rates of modification in the two states were significantly different. For A226C, the reaction rate using the open protocol could not be fit to a single exponential, consistent with different rates of modification in the resting and active states of S4. When the data were fit to two time constants, the fast component of the exponential was well-fit (Table 3-1, Fig 3-5); however, the error of the fit of the slower component was very large. To measure and accurately fit the slow component of the reaction and minimize modification in the active state, the closed protocol was used. Using this protocol, the reaction fit a single exponential (Fig 3-4 and Table 3-1), consistent with modification occurring primarily in the resting state. Comparing the two rates showed that A226C was modified 7.5-fold faster in the open protocol. In contrast to A226C, modification of I227C using both the open and closed protocols appeared to follow a single exponential time course (Fig. 3-4). Although a two exponential fit was expected, the similar rates of modification were not resolvable by mathematical fitting. Nonetheless, these results demonstrate that A226C and I227C are accessible to the extracellular solution when the S4 is at rest, but upon depolarization the residues are modified at a slightly faster rate.

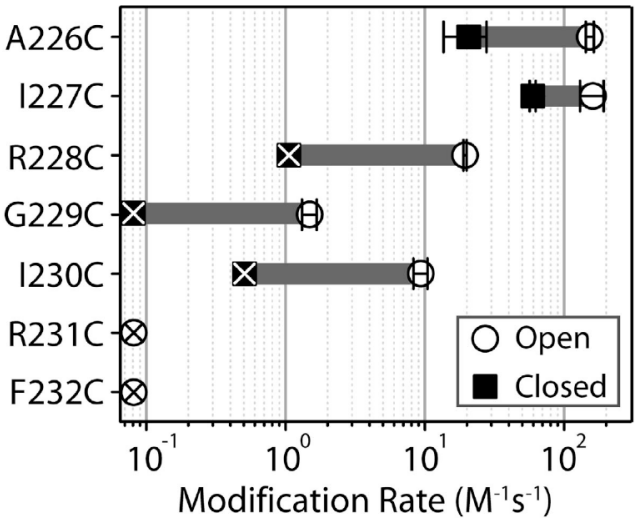

Figure 3-5 Comparison of MTSET modification rates for Q1 S4 cysteine substitutions

MTSET modification in the open protocol is represented by open circles, the closed protocol by filled squares. The gray bar indicates the fold-change in rate between the open and closed protocols. X-out open circles indicate no observed change in current using the open protocol; X-out squares are an estimate of reaction rate in the closed protocol based on the extent of modification determined by switching to the open protocol. Data were averaged from 3-6 oocytes ± SEM.

Table 3-1. Comparison of MTSET Modification of S4 residues in KCNQ1[1]

Construct	KCNQ1		KCNQ1/KCNE1		KCNQ1/KCNE3	
	k_{open}	k_{closed}	k_{open}	k_{closed}	k_{open}	k_{closed}
A226C	153 ± 10	21 ± 7*	11 ± 2	5.2 ± 0.3*	64 ± 5	23 ± 2*
I227C	161 ± 31	60 ± 3*	12 ± 3	13 ± 1	29 ± 3	26 ± 4
R228C	20 ± 1	~ 1	15 ± 1	~ 1	28 ± 3	19 ± 2*
G229C	1.5 ± 0.2	~ 0.1	0.49 ± 0.06	< 0.05	8.5 ± 1.0	5.3 ± 0.6*
I230C	9.4 ± 1.1	~ 0.5	1.2 ± 0.1	< 0.05	19 ± 2	15 ± 1

[1]Data from individual exponential fits in ND96, obtained from 3–7 oocytes, All MTSET modifications were fit to a single exponential, except for Q1(A226C) in the open protocol, which required a biexponential fit to extract the fast component of the reaction, as described in the Materials and Methods. k_{open} and k_{closed} are the second order modification rate constants ($M^{-1} \cdot s^{-1}$) determined using the open and closed pulse protocols. Measured values are mean ± SEM. Approximate values were calculated based on the extent of modification in the closed protocol, as described in the Materials and Methods. Statistical comparison is between k_{open} and k_{closed} for each mutant K^+ channel complex; *, $p < 0.05$.

MTSET modification of the three other S4 residues (R228C, G229C, I230C) could only be measured in the open protocol, but was well fit to a single exponential (Fig. 3-4). These residues were somewhat modified by MTSET in the "closed" protocol; however, the linear rate of modification was consistent with the reaction occurring during the short test depolarizations when the S4 is in the active state. Since the time course needed to complete the reaction in the closed protocol was not experimentally tractable (hours) with workable concentrations of MTSET, the extent of modification in the closed protocol was determined by switching to the open protocol after ~ 500 s. Normalization of the data using this end point allowed for comparison of the data generated from the two protocols (Fig. 3-4). Based on the extent of modification, the reaction proceeded in the closed protocol ~ 15–20 fold slower than in the open, which closely approximates the 18-fold difference in depolarization duration between the two protocols. Thus, these three S4 mutants (R228C, G229C, I230C) are only modified when the channel is in the depolarized state.

Measuring the rate of voltage sensor equilibration in Q1/E1 K^+ channel complexes

The next task was to determine whether these mutant Q1 channels would assemble with E1 to produce complexes with slowly activating kinetics and remain modifiable in a state-dependent manner. Co-expression of Q1 mutants (R228C, G229C, I230C) with E1 produced channel complexes that were highly reminiscent of wild-type Q1/E1, but after MTSET modification the mutant complexes became rapidly activating and open at negative potentials, as shown for R228C/E1 in Figure 3-6A.

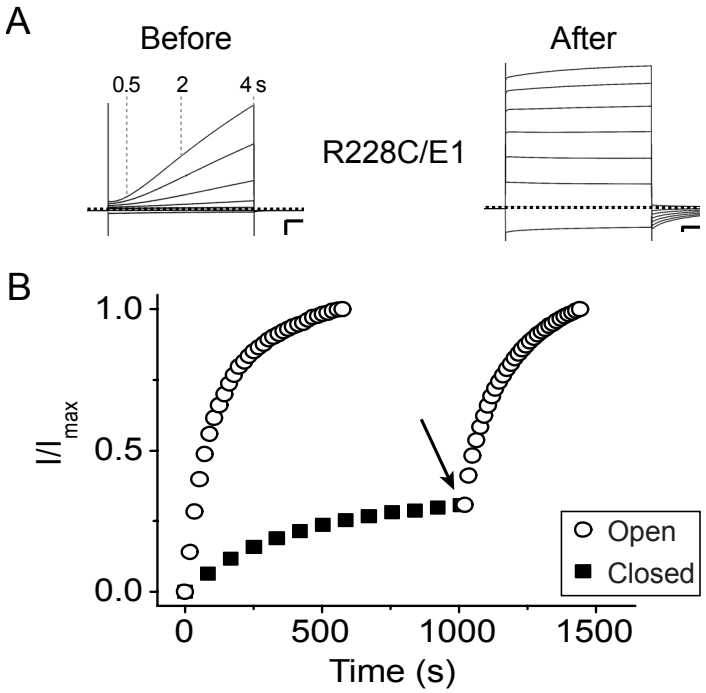

Figure 3-6 R228C/E1 complexes show state-dependent modification by MTSET

(A) TEVC recordings from R228C/E1 complexes expressed in *Xenopus* oocytes before and after MTSET modification. Oocytes were held at −80 mV and currents were elicited from 4-s command voltages from −100 mV to +40 mV in 20-mV increments. Gray dotted lines denote the amount of current from a 40-mV depolarization at 0.5, 2, and 4 s. Scale bars represent 0.5 μA (y-axis) and 0.5 s (x-axis). Dashed line indicates zero current.

(B) Change in current for R228C/E1 monitored over time using 40-mV test pulses with continuous perfusion of 400 μM MTSET. In the 'open' protocol (open circles), channels were depolarized 11% of the total time; 'closed' protocol (filled squares), 0.6% of total time. Shifting to the open protocol (arrow) after ~1000 s shows the completion of MTSET modification. Currents from the open and closed protocols were normalized to the maximal change in current for comparison.

MTSET modification was state-dependent for all three mutant Q1/E1 complexes (Table 3-1). Figure 3-6B shows that MTSET modification of R228C/E1 occurs rapidly in the open protocol, but using the closed protocol the mutant complex was modified very slowly, consistent with the reaction occurring primarily in the active state. To estimate the rate of modification in the closed protocol, the reaction was followed to completion after shifting from the closed to the open protocol (Fig. 3-6B, arrow). The observed increase in current was due to subsequent modification of unreacted cysteines in S4 and was not an artifact of changing the interpulse interval since it was only observed when MTSET was in the bath solution.

These three state-dependent Q1/E1 mutant complexes were then used to determine whether the slow gating in Q1/E1 complexes is due to S4 slowly transitioning from the resting to active state. If the slow activation observed in Q1/E1 complexes is due to a sluggish voltage sensor, the MTSET modification rate of the cysteines in S4 will decrease with shorter pulse durations as long as the opening of the intracellular gate itself does not alter S4 accessibility to MTSET. Conversely, if E1 has no effect on voltage sensor movement, then the modification rate should be independent of pulse duration. To experimentally test these two possibilities, the total depolarization time was kept constant (11%), but the individual pulse lengths were varied between 0.1 and 4 s. (Fig. 3-7, inset). The R228C/E1 mutant complex was examined first. Since a series of rapid, short pulses can cumulatively shift the S4 segments into the active state and give rise to an apparent increase in instantaneous conductance (Bett et al., 2006), the interpulse interval required to fully reset the voltage sensors was determined in the absence of MTSET (Fig 3-7 top).

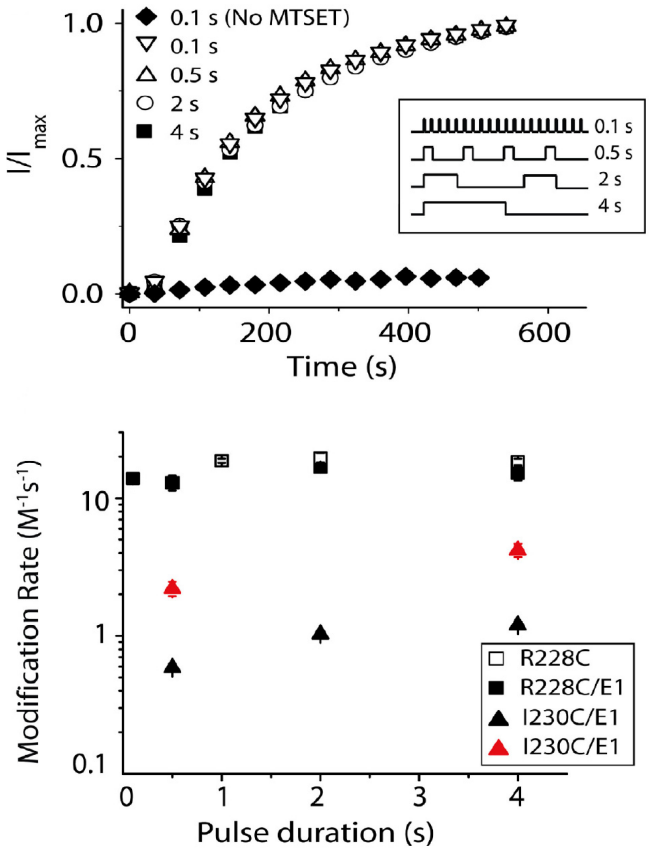

Figure 3-7 S4 voltage sensors reach equilibrium quickly in Q1/E1 complexes upon depolarization

(Top) Representative plots from the MTSET reaction with R228C/E1 using 0.1, 0.5, 2, or 4 s 40-mV pulses, where the total depolarization time was kept constant (inset). The total MTSET exposure time is plotted versus normalized current at the end of the depolarization. Filled diamonds indicate the interpulse interval required to reset voltage sensors between pulses when no MTSET was added (900-ms interval for 100-ms pulse).

(Bottom) Comparison of R228C, R228C/E1, and I230C/E1 in pulse duration experiments. Black symbols represent modification by MTSET, red symbols modification by MTSES. Data were averaged from 3-6 oocytes ± SEM.

MTSET treatment of R228C/E1 with different pulse durations from 0.1 to 4 s resulted in nearly identical rates of modification (Fig. 3-7). As a comparison, a similar set of pulse frequency experiments was performed on unpartnered R228C to determine if the rate of S4 modification in homotetrameric Q1 channels also remained constant with various pulse durations (Fig. 3-7, bottom). Similar pulse duration experiments with the G229C/E1 mutant complex were not experimentally feasible due to the extremely slow modification rate (Table 3-1). However, for I230C/E1, MTSET modification rates were modestly dependent on pulse duration. With 500 ms pulses, the rate of modification was ~ 2-fold slower than for 4 s pulses. A similar result was also obtained using the negatively charged MTS reagent, MTSES (Fig. 3-7, red triangles). Thus, the examination of the state-dependent Q1/E1 complexes in pulse duration experiments shows that the voltage sensors reach equilibrium quickly when E1 is present.

Voltage sensor equilibrium measurements in Q1/E3 K^+ channel complexes

Finally, Q1 voltage sensors were examined in the presence of E3. Co-expression of E3 with all but one of the S4 cysteine mutants resulted in functional complexes that were constitutively conducting and possessed rapid gating kinetics similar to wild-type Q1/E3 complexes (Fig. 3-8). The one deviant, R228C/E3, appeared to be closed at hyperpolarizing potentials and the depolarization-elicited currents were small in amplitude and slowly activating. Of these mutants, five were rapidly modified by MTSET and the reactions went to completion in both the closed and open protocols (Fig. 3-8).

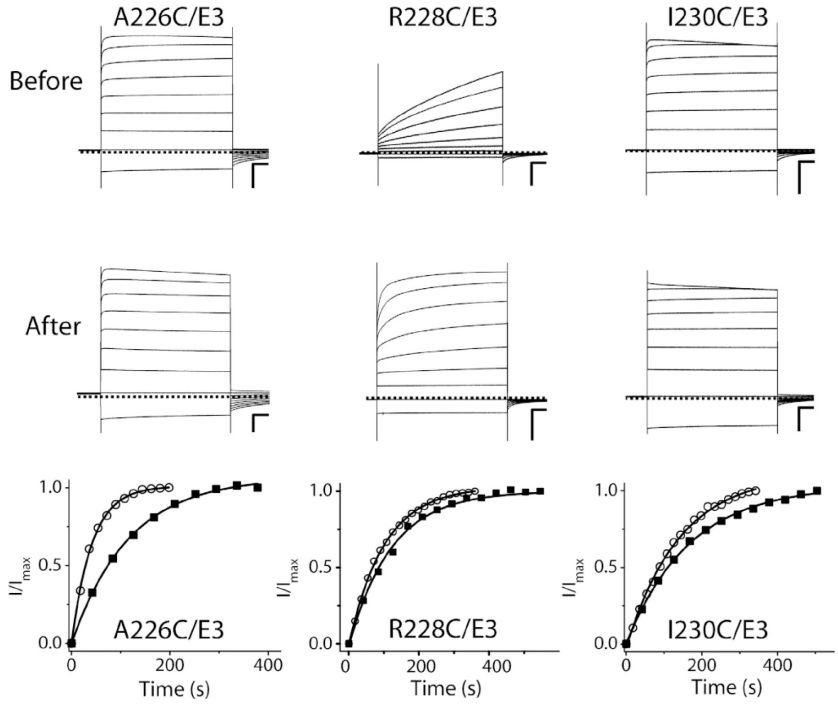

Figure 3-8 S4 cysteine substitutions in Q1/E3 complexes show state-independent modification

(Top) TEVC recordings from A226C/E3, R228C/E3 and I230C/E3 complexes expressed in *Xenopus* oocytes before and after MTSET modification. Oocytes were held at −80 mV and currents were elicited from 4-s command voltages from −100 to +40 mV in 20-mV increments. Scale bars represent 0.5 μA (y-axis) and 0.5 s (x-axis). Dashed line indicates zero current.

(Bottom) Change in current monitored over time using 40-mV test pulses with continuous perfusion of 400 μM MTSET. In the 'open' protocol (open circles), the channel complexes were depolarized 11% of the total time; 'closed' protocol (filled squares) 0.6% of total time. Currents from open and closed protocols were normalized to the maximal change in current for comparison. Curves were fit to monoexponential time courses and fitted parameters are presented in table 3-1.

Moreover, all MTSET reactions were pseudo-first order and well fit to single exponentials, indicating that the S4 residues in Q1/E3 complexes were readily accessible to the extracellular solution in both the closed and open protocols (Table 3-1). The lack of state-dependent modification for these S4 cysteine mutants when paired with E3 are in striking contrast to when the mutants were expressed alone, where A226C showed biexponential modification rates using the open protocol and R228C, G229C, and I230C were only modified upon depolarization (Fig. 3-4 & 3-5). The possibility that state-independent modification observed with Q1/E3 channels was due to the native extracellular cysteine in E3 was initially a concern. Although control experiments with wild type Q1/E3 complexes showed no measurable effect in the presence of MTSET, modification of this E3 cysteine will result in a disulfide bond, which could react with the cysteine mutants in S4 via an accelerated disulfide exchange reaction. To eliminate this possibility, experiments were repeated with a cysteine-less version of E3 and similar state independent modification of I230C's voltage sensors was obtained ($k_{open} \sim 15\ M^{-1}s^{-1}$, $k_{closed} \sim 14\ M^{-1}s^{-1}$). Examination of the deepest modifiable cysteine residue (I230C) with E3 at different test pulse potentials revealed that the rate of MTSET modification was independent of voltage from – 100 to 40 mV (Fig. 3-9). In total, these results argue that at hyperpolarizing potentials, the equilibrium of voltage sensors in Q1/E3 complexes is shifted such that they are significantly exposed to the extracellular solution.

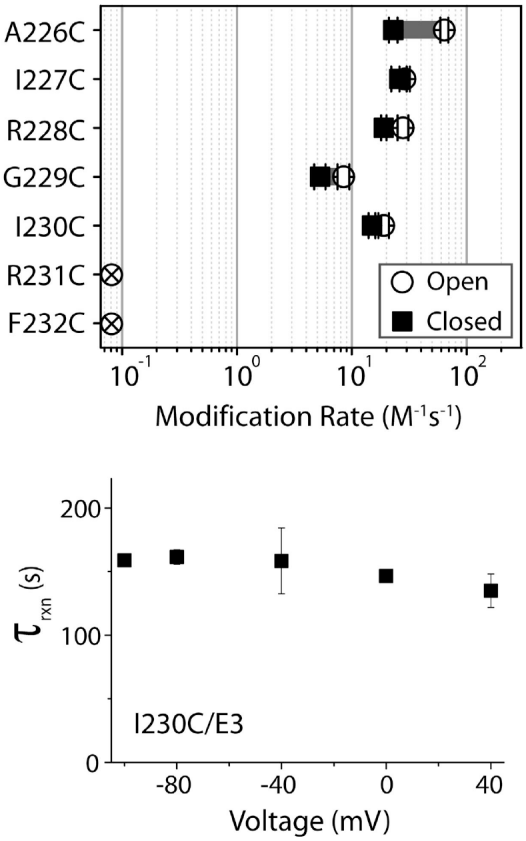

Figure 3-9 The equilibrium of voltage sensors is shifted to favor the active state in Q1/E3 complexes

(Top) Comparison of MTSET modification rates for Q1/E3 S4 cysteine substitutions in the open (open circles) or closed (filled squares) protocols. The gray bar gives the fold-change in rate between the open and closed protocols. X-out open circles indicate no observed change of current using the open protocol. Data were averaged from 3 to 5 oocytes ± SEM.

(Bottom) The rate of MTSET reaction with I230C/E3 channel complexes is independent of voltage. Oocytes were held at −80 mV, and for each voltage, 4-s pulses were followed by a −30 mV tail pulse (100ms), which was used to monitor the change in current upon MTSET application. The reaction time constant from single exponential fits is plotted for each voltage potential. Data were averaged from 3 to 4 oocytes ± SEM. One-way analysis of variance indicates that $p > 0.5$ for each data point in comparison to the others.

Discussion

MTSET accessibility of cysteine residues in the S4 segment of Q1 channels

This chapter examined the extracellular accessibility of introduced cysteines in the S4 voltage sensors of Q1 channel complexes to indirectly assess their position and equilibrium. Although this approach has faithfully mirrored more direct measurements of S4 whereabouts in other voltage-gated channels (with gating currents and fluorescently labeled voltage sensors), there are at least three caveats to consider. First, accessibility measurements may not exclusively report on S4 movement since other K^+ channel rearrangements could expose S4 to the extracellularly applied reagent. Second, since modification is ascertained by measuring changes in macroscopic current, it is unclear how many modified S4 segments are required to produce the measured effect. Third, MTS-modified cysteines can undergo disulfide exchange with nearby free sulfhydryls, which may affect the rate and magnitude of the measurement.

Using MTSET as the accessibility reagent, modification was observed for cysteines introduced at positions 226–230 in the S4 of Q1 channels. The measured MTSET modification rates were slower compared to voltage sensors in other channels as well as model thiols (Larsson et al., 1996; Karlin and Akabas, 1998). Although voltage-gated channels share a common protein fold, differences in the microenvironments (steric and electrostatic) surrounding the S4 segment could explain the slow reaction rates observed with Q1. To further elucidate the influence of the Q1 protein environment on S4's range of motion, examination of the intracellular accessibility to MTSET would be particularly informative. Unfortunately, the current from Q1 channel complexes in

excised macropatches rapidly decreases over time (rundown) (Loussouarn and Escande, 2003), preventing the use of this experimental technique.

External MTSET modification also revealed that the voltage sensors in Q1 channels are sensitive to the removal, introduction, and specific location of charges in the S4 segment. Removal of the positive charge at residues 228 and 231 by cysteine substitution ablated activation kinetics, as was previously observed with alanine mutants at these same positions (Panaghie and Abbott, 2007). Charge re-introduction by MTSET modification restored gating kinetics and increased current output for R228C. However, introduction of positive charge at previously uncharged positions resulted in channels with nearly instantaneous activation kinetics for all modifiable cysteine mutants except I230C. Thus, the charge-sensitivity of the Q1 S4 segment makes the effects of MTSET modification on the voltage-dependence and changes in current amplitude unpredictable. In contrast, the state-dependence of MTSET modification of the S4 cysteine residues in Q1 followed a clear pattern. The more N-terminal and presumably more accessible S4 residues were measurably modified in both the open and closed states. Correspondingly, modification of the more C-terminal residues was not detected, suggesting that these residues are too buried to react with MTSET. The remaining three residues (R228C, G229C, I230C) were strongly state-dependent and therefore used to examine the effects of E1 and E3 on voltage sensor equilibrium.

E1 does NOT appreciably slow the equilibration rate of the Q1 voltage sensor

Co-expression of E1 with the three state-dependent Q1 mutants resulted in two different rates of MTSET modification: R228C/E1 was modified at a similar rate as R228C alone whereas the modification of G229C and I230C was considerably reduced (~ 10-fold) in the presence of E1 (Table 3-1). While it is tempting to compare the absolute rates of MTS modification between Q1 and Q1/E1 channel complexes to determine whether E1 slows the voltage sensors, this measurement reports on the equilibrium of the voltage sensor and not the kinetics of movement. Thus, Nakajo and Kubo's conclusion that E1 peptides slow the transition of the S4 segment to the active state based on differences in MTS modification rates was premature (Nakajo and Kubo, 2007). Moreover, the inclusion of KCNE peptides in the Q1 complex adds the potential for steric and electrostatic interactions that could substantially reduce or enhance the rates of MTS modification. Therefore, it is imperative to examine each individual complex to elucidate the effects of KCNE peptides on voltage sensor equilibration rates. Accordingly, the dependence of MTSET modification rate on pulse duration was measured in an attempt to extract the kinetics of voltage sensor movement in Q1/E1 complexes.

Examining two of the strongly state-dependent S4 cysteine mutants revealed that R228C/E1 was modified independent of pulse duration (as short as 100 ms) whereas I230C/E1 modified somewhat slower with the shortest depolarizations. For R228C/E1, this result implies that voltage sensors reach equilibrium in less than 100 ms and that the rate limiting step is the opening of the Q1/E1 activation gate. In support of this model, a

recent report found that the rate of A226C/E1 modification by MTS reagents is also independent of pulse duration with pulses as short as 30 ms (Nakajo and Kubo, 2007). For I230C/E1, a 2-fold difference in modification rate was observed between the 500 ms and 4 s pulse durations using both MTSET and MTSES. However, this difference does not fully account for the ~ 7-fold change in conductance observed over this time frame, and may be attributed to increased extracellular exposure of this residue induced by cytoplasmic gate opening or other delayed conformational changes. Alternatively, if E1 does partially slow voltage sensor equilibration, the lack of dependence on pulse duration for R228C/E1 (and A226C/E1) can be explained by two pairs of voltage sensors moving at different rates. To directly measure these rates, it will require either measuring gating currents or monitoring S4 motions with reporter probes. Both of these experimental approaches will be challenging since the S4 segment is charge-poor and its modification with cysteine-specific reagents (at least MTSET) typically abolishes Q1 channel gating.

E3 shifts the voltage sensor equilibrium to favor the active state

For Q1/E3 complexes, the entire panel of S4 cysteine mutants was modified by MTSET in the closed protocol, indicating that these residues are equally accessible to the reagent at resting and depolarizing potentials (Table 3-1). Although the increase in reactivity for a single mutant could be attributed to local accessibility differences between Q1 and Q1/E3 channel complexes, the across-the-board loss of state-dependence strongly argues that the voltage sensor equilibrium in Q1/E3 complexes is shifted to favor the active state at hyperpolarizing potentials. This result confirms that the tight linkage

between voltage sensor and activation gate, which has been observed in the majority of wild-type voltage-gated channels, is maintained in Q1/E3 complexes. This differs from mutagenic investigation of activation gates and voltage sensors in other voltage-gated channels that abolish this link, uncoupling the coordinated movement of these two protein domains (Lu et al., 2002; Sukhareva et al., 2003). Since Q1/E3 complexes exhibit some voltage-dependence, this would suggest that E3 does not lock the voltage sensors up, but enables voltage-independent access to the active state. A recent mutagenic investigation of KCNQ channel voltage sensors suggests that E3 converts Q1 into a leak channel because the S4 segment has a smaller net positive charge (+3) compared to the other members in the family (Panaghie and Abbott, 2007). For most of the cysteine modifications examined here, adding an additional positive charge to the S4 with MTSET converted Q1 channels and Q1/E1 complexes into voltage-independent leak channels. This trend appears to contradict the requirement for a charge-poor S4 to induce a leak current. However, the resultant disulfide bonded ethyltrimethylammonium is a terrible structural mimic of arginine or lysine. Moreover, the haphazard attachment of positive charge to the S4 could also disrupt voltage-sensing since the spacing of charges in voltage-sensitive channels is also highly conserved (Catterall, 1988). On the other hand, one MTSET modification supports the paucity of charge model proposed by Abbott and co-workers. Unmodified R228C/E3 complexes afforded small currents that were only measurable at positive potentials (Fig. 3-8); however, reinstating the charge at position 228 with MTSET afforded robust currents with more Q1/E3 character.

Conclusions

The discovery that E1 and E3 differently influence the motions of Q1 channels supports a bipartite model previously proposed for KCNE modulation of Q1 channels (Gage and Kobertz, 2004). This model proposed that the E3 transmembrane domain was dominant in modulation and overrides the conserved C-terminal domain of KCNE peptides, whereas the E1 transmembrane domain was passive in modulation, allowing the C-terminus to influence channel gating. These new data suggest that the mechanism for bipartite modulation arises from the tight coupling of the voltage sensor position to the activation gate. The E3 transmembrane domain shifts the voltage sensor equilibrium to favor the active state, resulting in a predominately open activation gate. Moreover, since E1 does not appreciably slow the rate of voltage sensor equilibration, it would allow the cytoplasmic domain of E1 to slow activation gate opening. Although these data support the bipartite model and suggest potential Q1/KCNE protein-protein interactions, future structure-function studies are needed to determine whether the modulatory effects of KCNE peptides on voltage sensors and activation gates occur via a direct or allosteric mechanism.

CHAPTER IV: Discussion and Future Directions

This thesis examined the nature of Q1 modulation by two homologous yet distinct β-subunits: E1 and E3. Q1/E1 complexes activate very slowly in a voltage-dependent manner whereas Q1/E3 channels activate almost instantaneously, generating currents with a voltage-independent component even at negative voltages. These dramatically different effects prompted this investigation into the secondary structure of E1's C-terminus and the impact of E1 and E3 subunits on Q1 voltage sensor equilibrium.

Although the C-terminal region, in particular, is well conserved in E1 and E3 peptides, its influence on channel modulation is markedly different. The bipartite model explains two distinct sites of channel modulation residing in the transmembrane domain and C-terminus (Gage and Kobertz, 2004). In E1, a permissive transmembrane domain allows C-terminal modulation to dominate as the deletion of membrane-abutting C-terminal residues remove E1's modulatory effect. Also, several long-QT mutations in this region further highlight its importance (Splawski et al., 2000).

Chapter II addressed the individual contributions of membrane-abutting C-terminal residues in E1. Using perturbation mutagenesis, a number of positions were identified that substantially alter channel gating when mutated to alanine or leucine. These mutations clustered onto a single protein interface with helical structure that is kinked at proline 77. In support of this finding, the same E1 residues suggested to interact with the Q1 channel complex were recently shown to form crosslinks with residues in the cytoplasmic-facing pore region of Q1 (Gage, 2008).

Although many studies have addressed the regions in E1 and E3 that interact with or modulate Q1 channels, fewer groups have examined the effects of these peptides on the structure and function of Q1. The voltage sensor is an appealing target because of the extreme effects that E1 and E3 have on voltage-dependent gating. Abbott and coworkers proposed that the paucity of charge in Q1's S4 segments contribute to its sensitivity to such extreme modulation – the nature of which is not seen in other Kv channels that assemble with these same β-subunits (Panaghie and Abbott, 2007).

Chapter III elucidated the response of Q1 voltage sensor equilibrium to assembly with E1 or E3. Cysteine accessibility experiments were performed to identify positions in the S4 segment of Q1 that could be modified by MTSET only when voltage sensors were active. In Q1/E1 channels, the rate of modification for these state-dependent cysteine mutants was not dependent on pulse length, indicating that voltage sensors equilibrate quickly and are not responsible for the slow gating observed for these channels. Cysteines examined in Q1/E3 complexes showed state- and voltage-independent modification by MTSET, confirming that voltage sensors are shifted to favor the active state causing constitutive current conduction.

This work reinforces the importance of the E1 transmembrane-abutting C-terminus in producing the slowly activating I_{Ks} currents that are vital to maintaining heart rhythmicity. This thesis also explains the distinct influences of E1 and E3 on Q1 voltage sensing.

Future Directions

A number of questions remain unanswered regarding the nature of unique modulation endowed by E1 and E3. Melman and colleagues suggested that E1 and E3 may interact with the Q1 pore in slightly different ways (Melman et al., 2004). It is possible that Q1/KCNE interactions are state-dependent such that their interaction surface shifts when the channel moves from the closed to open conformation. By docking their recent NMR structure of E1 onto a Q1 model, the Sanders group suggests that E1 may interact with two different clefts of Q1 depending on channel conformation (Kang et al., 2008). The crystal structure that best approximates Q1 is the mammalian Kv1.2, which indeed shows a gap between each VSD and its neighbor (Long et al., 2005a), suggesting an ideal location for E1 to interact with the pore as well as the voltage sensor. A similar structural model is proposed by combining data showing disulfide bond formation between cysteines introduced in the E1 N-terminus and either Q1's S4 (Nakajo and Kubo, 2007) or state-dependent disulfide bonds with S1 (Xu et al., 2008). This model places E1 between two VSDs, where it interacts with the S4 helix of one subunit on one side, the S1 helix of a second subunit on the other side, and the S6 pore-lining helix of a third subunit that sits between the two VSDs. Interacting points between C-terminal residues of E1 with Q1 that are implied in Chapter II and have been verified through crosslinking experiments (Gage, 2008) may further constrain the position of E1 within this model; however, assessing the state dependence of these interactions is crucial before any definitive determinations can be made.

It is also possible that the structure of E1 is influenced by interactions with Q1. The kinked α-helical conformation proposed for the proximal C-terminal domain of E1 in Chapter II was not observed in the NMR solution structure of E1 determined in lipid micelles (Kang et al., 2008). This discrepancy can be explained by the fact that the NMR structure was solved for E1 alone, in the absence of the Q1 channel, and therefore does not account for interactions between Q1 and E1 that may stabilize a kinked helical conformation. Also, the globular micelle environment does not accurately replicate a planar membrane bilayer and may introduce additional structural distortions. Although indirect, perturbation mutagenesis may be a superior measure of E1 structure since this technique measures functioning, assembled channels in a native-like membrane.

What role does the conserved C-terminal domain play in other KCNE β-subunits? The bipartite model predicts that this region is not required for basal activation in Q1/E3 complexes, and accordingly, introducing the dominant negative D76N mutation into the corresponding location in E3 (D90N) has no measurable effect on channel gating (Gage and Kobertz, 2004). In contrast, the C-terminus is required for E4 inhibition of Q1 channels. Chimeras that replace the C-terminus of either E1 or E3 with that of E4 inhibit Q1 channel activity similar to wild type E4, and introduction of the E1 C-terminus into E4 abolishes this inhibition (Manderfield et al., 2008). The emerging theme extends the bipartite model to include the entire KCNE family: the transmembrane domains of E3 and probably E2 are required for basal activation of Q1 and C-terminal contributions from these β-subunits are masked. Conversely, E1, E4, and perhaps E5 all contain permissive transmembrane domains which unveil C-termini that are critical for delayed,

and sometimes, inhibited Q1 channel activation. Although this model has not yet been tested on E5, similar chimera constructions and perturbation mutagenesis strategies could be employed to dissect which domains and residues cause slow gating and the large voltage-activation shift. The challenge in performing these experiments is the extremely positive depolarizations required to elicit measurable current from Q1/E5 complexes.

Chapter III reveals that voltage-independence in Q1/E3 complexes occurs because voltage sensors are shifted to favor the active state. However, are all four voltage sensors equally shifted? It is possible that if two E3 β-subunits assemble with each Q1 channel, their interaction causes only two voltage sensors to shift 'up' at negative voltages. Since MTS-modification of cysteines introduced in Q1's S4 cannot discriminate how many S4 cysteines must be modified to produce a measurable current increase, this question remains unanswered. The tethered charybdotoxin approach employed to count two E1 β-subunits in functioning Q1/E1 complexes (Morin and Kobertz, 2008) could also resolve the number of E3 β-subunits in Q1/E3 complexes (Figure 4-1). This technology could then be extended to count the number of shifted voltage sensors in Q1/E3 complexes at negative voltages by modifying cysteines introduced in the S4 domain instead of the β-subunits.

Just as derivitized scorpion toxins have been used to probe the extracellular side of functioning K^+ channels, a similarly derivitizable protein may be valuable to examine channel gating from the intracellular perspective. Since Q1 channels rapidly lose current

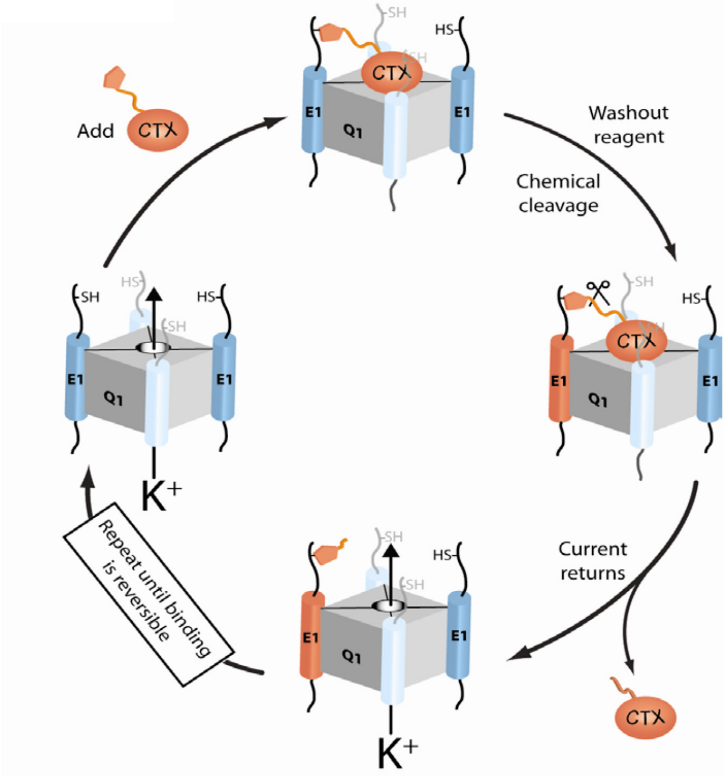

Figure 4-1 Cartoon depicting one modification cycle used to count the number of E1 subunits in Q1/E1 complexes using a derivatized charybdotoxin (CTX)

The CTX reagent is added (top left) and irreversibly blocks channels by tethering its maleimide moiety to the thiol group of a cysteine introduced into the N-terminus of E1. The reagent cannot be washed out without chemical cleavage (top right), which then allows the CTX blocking moiety to diffuse away. The E1 cysteine is then permanently modified and no longer reactive to further rounds of modification. Therefore, the number of E1 peptides in the channel complex is simply the number of cycles that require the tethered reagent to be chemically cleaved for current to be restored. Figure 4-1 is from (Morin and Kobertz, 2008).

(rundown) in excised patches (Loussouarn and Escande, 2003), access to the intracellular aspects of this protein's function have been limited. To build on the work presented in useful. One approach to monitor the motions of the intracellular gate would be to use the calmodulin protein as a fluorescent sensor of gate position. Calmodulin constitutively binds the Q1 C-terminus very close to the S6 gate (Ghosh et al., 2006; Shamgar et al., 2006), and many years of studying this small, soluble protein reveal straightforward methods for its mutagenesis, purification, and labeling with a number of cysteine-reactive probes (Allen et al., 2004). To use calmodulin as a fluorescent sensor of intracellular gate position requires a fluorophore that changes in fluorescence intensity when the channel gate moves from the open to closed conformation. If the microenvironment surrounding the channel gate is sufficiently different in the open versus closed conformation, a solvatochromatic fluorophore may be useful. Otherwise, a fluorophore that undergoes self-quenching or self-FRET may be appropriate. Preliminary data (Appendix) indicate that this type of experiment may be feasible; however the exact details are still under investigation. In all, the use of derivatized calmodulin as a tool to probe the intracellular side of Q1/KCNE complexes using fluorescence, chemical biology or other methods remains a promising avenue.

Conclusion

In conclusion, this thesis adds to the growing body of biophysical and structure-function data describing the remarkably different ways that the small KCNE β-subunits modulate the gating and voltage sensing properties of the physiologically diverse KCNQ1 K^+ channel. Continuing studies will, no doubt, increase our understanding of how these fascinating channel complexes assemble, traffic, and function, and will expand the tools available to target deleterious channel dysfunction.

APPENDIX: Calmodulin as a Sensor of Intracellular Gate Motions in Q1/E1 K^+ Channel Complexes

KCNE subunits have very different effects on Q1 K^+ channel gating and voltage sensing. In the slowly activating Q1/E1 complexes, active voltage sensors are externally accessible within hundreds of milliseconds of depolarization, whereas channel activation continues over a much longer timescale of several seconds. This suggests that voltage sensor movement is not the rate-limiting step in channel activation, and implies a slowly moving intracellular gate. Calmodulin is a small (17 kD), soluble signaling protein that constitutively binds the Q1 C-terminal region in close proximity to the S6 gate. To demonstrate that calmodulin may be used as an intracellular sensor of Q1/E1 gating motions, a cysteine-containing calmodulin mutant was purified, derivatized, and shown to assemble with Q1 channels in *Xenopus* oocytes. This preliminary evidence suggests a novel means to probe the intracellular side of a functional ion channel in living cells by modifying one of its soluble partner proteins.

Materials and Methods

Mutagenesis, protein expression and purification: Calmodulin (CaM) DNA was obtained from David Yue (Johns Hopkins) and was subcloned into the pET-DUET1 vector for expression and purification. The T35C point mutant was introduced by Quikchange site-directed mutagenesis (Strategene) and confirmed by DNA sequencing of the entire gene. Recombinant CaM-T35C was expressed and purified according to the protocol by Hayashi and others (Hayashi et al., 1998). The pET-DUET1 plasmid containing CaM-T35C (~200 ng) was used to transform *E. Coli* strain BL21 (DE3). CaM-T35C was expressed by induction with 0.4 mM isopropyl-β-D-thiogalactoside (IPTG) once A_{595} reached 1.0. The culture was grown for an additional 8 hours post induction, and pellets were collected by centrifugation at 5000 rpm for 15 minutes at 4°C. The bacterial pellet was resuspended in 50 mM Tris-HCl buffer, pH 7.5, containing 2 mM EDTA, 0.2 mM phenylmethanesulfonyl fluoride (PMSF) and 1mM 2-mercaptoethanol. Cells were lysed using a Microfluidizer Cell-disrupter (Microfluidics Corp, Newton, MA) and centrifuged at 15000 rpm for 15 minutes at 4°C. After addition of 5 mM $CaCl_2$, the supernatant was applied to a phenyl-Sepharose CL-4B column equilibrated with 50 mM Tris-HCl, pH 7.5, 5 mM $CaCl_2$, and 0.1 M NaCl. After washing until A_{280} reached baseline, proteins were eluted using 50 mM Tris-HCl pH 7.5, 1mM EGTA. Fractions containing CaM were dialyzed against distilled water and lyophilized. The concentration of resuspended CaM solutions was determined by ninhydrin assay (Rosen, 1957).

Calmodulin labeling: Purified CaM-T35C (200 nmoles) was resuspended in PBS and reduced with 5 mM DTT for 30 minutes. Maleimide PE02-Biotin (Pierce) was added at 20 molar excess, and the mixture incubated at room temperature for 2 hours. The reaction mixture was then dialyzed against PBS (3 solution changes, 500 mL each) using a 10,000 molecular weight cutoff Slidalyzer (Pierce) overnight at room temperature to remove unreacted Maleimide reagent.

Oocyte preparation and electrophysiology: Oocytes were surgically removed from Xenopus laevis and defolliculated using 2 mg/mL collagenase (Worthington Biochemical Corp.) in OR2 containing (mM): 82.5 NaCl, 2.5 KCl, 1 $MgCl_2$, 5 HEPES, pH 7.4 for 75-90 min. Isolated oocytes were rinsed with and stored in ND96 bathing solution (ND96B) containing (mM): 96 NaCl, 2 KCl, 1.8 $CaCl_2$, 1 $MgCl_2$, 5 HEPES, 50 μg/mL gentamicin (Sigma-Aldrich), pH 7.4 at 18°C. Approximately 24 h after extraction, oocytes were microinjected with 27.6 nL total volume of cRNA and/or protein containing Q1 (7.5 ng/oocyte) and CaM (0.5 μmoles or 5 μmoles/oocyte). After 3–6 days, currents were recorded using Warner Instrument OC-725C two-electrode voltage clamp (TEVC) and the data were acquired with Digidata 1322A using pClamp 8 or 9 (Axon Instruments). Electrodes were filled with 3 M KCl, 5 mM EGTA, 10 mM HEPES, pH 7.6, and had resistance between 0.2 and 1.0 MΩ. For each experiment, oocytes were held at – 80 mV in ND96 (in mM): 96 NaCl, 2 KCl, 0.3 $CaCl_2$, 1 $MgCl_2$, 5 HEPES, pH 7.4, and pulsed to a command potential of 40 mV.

Oocyte membrane preparation: A sample of oocytes injected with Q1 only, Q1 and CaM-B or CaM-B only were checked for functional K^+ currents three days after injection. Each batch of oocytes was homogenized at 4°C in 0.9 mL homogenization buffer: 100 mM HEPES, pH 7.6, 1 mM EDTA, 50 mM DTT, and 100 μg/mL phenylmethanesulfonyl fluoride (PMSF). Cell debris was pelleted by centrifugation at 3000 rpm for 10 minutes at 4°C and the supernatant was collected. The pellet was resuspended in 0.9 mL homogenization buffer and centrifuged once more (3000 rpm, 10 minutes, 4°C). The supernatants were combined and overlaid on a 15% sucrose cushion, prepared with 100 mM HEPES, pH 7.6. Samples were ultracentrifuged at 44,000 rpm for 75 minutes, and pelleted membranes were solubilized in immunoprecipitation reaction buffer containing 50 mM Tris-HCl, pH 7.4, 150 mM NaCl, 1 mg/mL BSA, 50 mM NaF, 5 mM EDTA, 1% Triton X-100, protease inhibitor cocktail.

Immunoprecipitation Analysis: After resuspending oocytes membranes in immunoprecipitation reaction buffer for ~ 2 hours at 4°C, insoluble material was pelleted by centrifugation at 14000 rpm for 1 minute at 4°C. Samples were incubated with 5 μl anti-Q1 antibody (Santa Cruz Biotechnology, Inc.) overnight at 4°C. The samples were bound to protein G beads (Pierce) for 2 hours at room temperature to separate antibody-bound protein complexes from oocytes membranes. The beads were washed twice with immunoprecipitation reaction buffer and once with detergent-free wash buffer. Co-immunoprecipitated proteins were eluted from the beads with SDS-gel loading buffer for 5 minutes at 95°C. One-fifth of the total input used for co-immunoprecipitation and

eluted proteins were resolved by SDS-PAGE and analyzed by Western blot with anti-biotin antibody (Sigma).

Results and Discussion

Calmodulin (CaM) is a small, soluble protein that constitutively binds the C-terminus of each Q1 subunit very close to the S6 gate (Ghosh et al., 2006; Shamgar et al., 2006), suggesting that calmodulin may be used as a sensor to probe the motions of the intracellular gate in Q1/E1 channel complexes. To determine if purified, derivatized calmodulin can assemble with functioning Q1 channel complexes inside living cells, the *Xenopus* oocyte expression system was used. Oocytes are ideal for this type of approach since purified protein can be directly injected into oocytes along with channel-encoding mRNA (Maduke et al., 1998); however, the purified, derivatized calmodulin must successfully assemble with Q1 channels at the plasma membrane without disrupting complex function.

Although calmodulin contains no native cysteines, cysteine-containing constructs have been previously generated and labeled for fluorescence resonance energy transfer (FRET) experiments (Allen et al., 2004). Therefore, one of the positions known to tolerate cysteine substitution and further fluorescent labeling, T35, was mutated to cysteine, over-expressed in *E. Coli* and purified (Figure A-1). To determine if CaM-T35C affects Q1 channel function, the purified protein was injected along with mRNA encoding Q1 into *Xenopus* oocytes. Figure A-2 shows that currents elicited from oocytes containing Q1 and CaM-T35C are indistinguishable from Q1 alone.

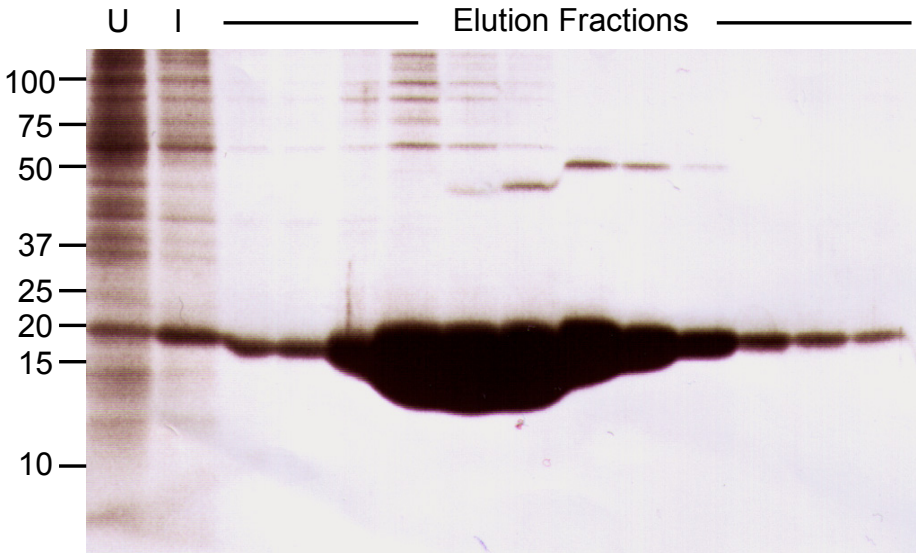

Figure A-1 Overexpression and Purification of Calmodulin T35C

SDS Polyacrylamide Gel Electrophoresis of total *E. Coli* BL21 (DE3) proteins before induction (U) and after IPTG-induction (I) followed by elution fractions from phenyl sepharose purification of recombinant calmodulin protein with the T35C mutation (~17 kD).

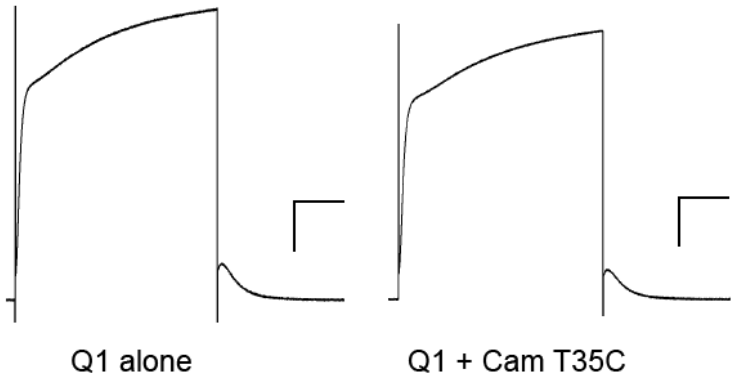

Figure A-2 Co-injection of purified Calmodulin T35C does not disrupt Q1 function

Two-electrode voltage clamp recordings of Q1 expressed alone (left) or in the presence of 5 μmoles purified Calmodulin T35C (right) expressed in *Xenopus* oocytes. Currents were elicited using a 4-s depolarization from − 80 mV to 40 mV. Scale bars represent 1μA (y-axis) and 0.5 s (x-axis).

Purified CaM-T35C was then labeled with biotin-maleimide and co-injected with Q1 in *Xenopus* oocytes. Figure A-3 shows that biotinylated calmodulin (~ 17 kD) co-immunoprecipitates with Q1 from purified oocyte membranes only when both Q1 and biotinylated calmodulin are injected.

This preliminary data confirms the ease with which cysteines can be introduced into calmodulin and labeled with maleimide-containing probes. Labeled calmodulin can assemble with Q1 in oocytes; however, it is still not clear whether labeled calmodulin out-competes the native *Xenopus* calmodulin for assembly with Q1. The reverse co-immunoprecipitation (IP α-biotin, IB α-Q1) combined with quantifying the amount of Q1 remaining in supernatants following biotin-pull down would suggest the fraction of Q1 that associates with biotinylated calmodulin in the membrane.

Although this work provides evidence to support the use of calmodulin as an intracellular probe, further study is needed to address whether fluorescence methods or a chemical biological approach would be the most effective means of implementation.

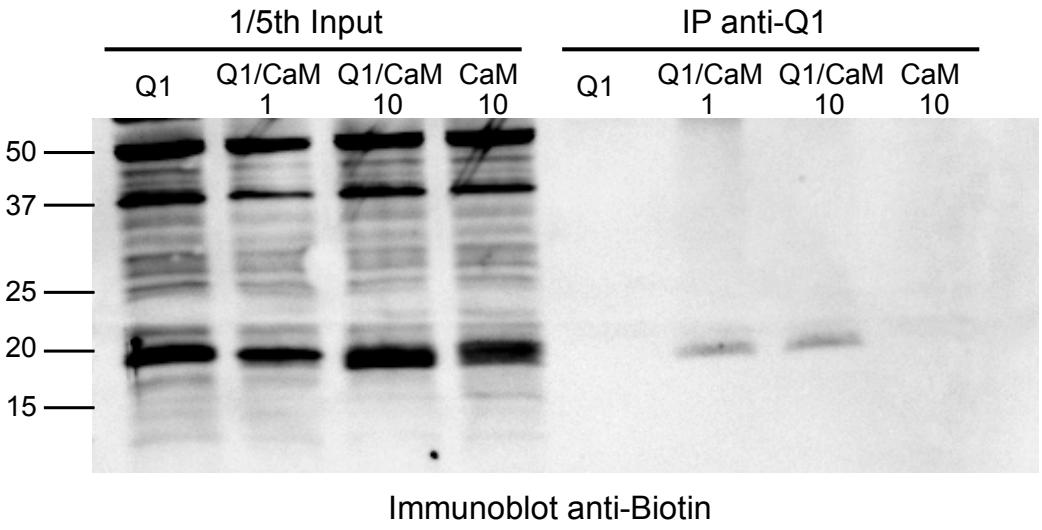

Figure A-3 Biotinylated Calmodulin co-immunoprecipitates with Q1 from *Xenopus* oocyte membranes

Co-immunoprecipitation of biotinylated calmodulin (~17 kD) with anti-Q1 antibody. Membranes from oocytes injected with either Q1 alone, Q1 with 0.5 μmoles of purified biotinylated calmodulin (Q1/CaM 1), Q1 with 5 μmoles of purified biotinylated calmodulin (Q1/CaM 10) or just 5 μmoles purified biotinylated calmodulin (CaM 10) were incubated with anti-Q1 antibody. One-fifth of the total detergent solubilized membranes and the precipitates were analyzed by SDS-PAGE and Western analysis was performed using anti-biotin antibody.

Bibliography

Abbott, G.W., Butler, M.H., Bendahhou, S., Dalakas, M.C., Ptacek, L.J. and Goldstein, S.A. 2001. MiRP2 forms potassium channels in skeletal muscle with Kv3.4 and is associated with periodic paralysis. *Cell*. 104:217-231.

Abbott, G.W., Butler, M.H. and Goldstein, S.A. 2006. Phosphorylation and protonation of neighboring MiRP2 sites: function and pathophysiology of MiRP2-Kv3.4 potassium channels in periodic paralysis. *Faseb J*. 20:293-301.

Abbott, G.W., Sesti, F., Splawski, I., Buck, M.E., Lehmann, M.H., Timothy, K.W., Keating, M.T. and Goldstein, S.A. 1999. MiRP1 forms IKr potassium channels with HERG and is associated with cardiac arrhythmia. *Cell*. 97:175-187.

Aggarwal, S.K. and MacKinnon, R. 1996. Contribution of the S4 segment to gating charge in the Shaker K+ channel. *Neuron*. 16:1169-1177.

Ahern, C.A. and Horn, R. 2005. Focused electric field across the voltage sensor of potassium channels. *Neuron*. 48:25-29.

Allen, M.W., Urbauer, R.J., Zaidi, A., Williams, T.D., Urbauer, J.L. and Johnson, C.K. 2004. Fluorescence labeling, purification, and immobilization of a double cysteine mutant calmodulin fusion protein for single-molecule experiments. *Anal Biochem*. 325:273-284.

Angelo, K., Jespersen, T., Grunnet, M., Nielsen, M.S., Klaerke, D.A. and Olesen, S.P. 2002. KCNE5 induces time- and voltage-dependent modulation of the KCNQ1 current. *Biophys J*. 83:1997-2006.

Armstrong, C.M. 1966. Time course of TEA(+)-induced anomalous rectification in squid giant axons. *J Gen Physiol*. 50:491-503.

Armstrong, C.M. 1969. Inactivation of the potassium conductance and related phenomena caused by quaternary ammonium ion injection in squid axons. *J Gen Physiol*. 54:553-575.

Armstrong, C.M. 1971. Interaction of tetraethylammonium ion derivatives with the potassium channels of giant axons. *J Gen Physiol*. 58:413-437.

Armstrong, C.M. and Bezanilla, F. 1973. Currents related to movement of the gating particles of the sodium channels. *Nature*. 242:459-461.

Armstrong, C.M. and Bezanilla, F. 1974. Charge movement associated with the opening and closing of the activation gates of the Na channels. *J Gen Physiol*. 63:533-552.

Barhanin, J., Lesage, F., Guillemare, E., Fink, M., Lazdunski, M. and Romey, G. 1996. K(V)LQT1 and lsK (minK) proteins associate to form the I(Ks) cardiac potassium current. *Nature*. 384:78-80.

Bendahhou, S., Marionneau, C., Haurogne, K., Larroque, M.M., Derand, R., Szuts, V., Escande, D., Demolombe, S. and Barhanin, J. 2005. In vitro molecular interactions and distribution of KCNE family with KCNQ1 in the human heart. *Cardiovasc Res*. 67:529-538.

Bett, G.C., Morales, M.J., Beahm, D.L., Duffey, M.E. and Rasmusson, R.L. 2006. Ancillary subunits and stimulation frequency determine the potency of chromanol 293B block of the KCNQ1 potassium channel. *J Physiol*. 576:755-767.

Bezanilla, F. 2006. The action potential: from voltage-gated conductances to molecular structures. *Biol Res*. 39:425-435.

Bianchi, L., Shen, Z., Dennis, A.T., Priori, S.G., Napolitano, C., Ronchetti, E., Bryskin, R., Schwartz, P.J. and Brown, A.M. 1999. Cellular dysfunction of LQT5-minK mutants: abnormalities of IKs, IKr and trafficking in long QT syndrome. *Hum Mol Genet*. 8:1499-1507.

Catterall, W.A. 1988. Structure and function of voltage-sensitive ion channels. *Science*. 242:50-61.

Cha, A., Snyder, G.E., Selvin, P.R. and Bezanilla, F. 1999. Atomic scale movement of the voltage-sensing region in a potassium channel measured via spectroscopy. *Nature*. 402:809-813.

Chanda, B., Asamoah, O.K., Blunck, R., Roux, B. and Bezanilla, F. 2005. Gating charge displacement in voltage-gated ion channels involves limited transmembrane movement. *Nature*. 436:852-856.

Chandrasekhar, K.D., Bas, T. and Kobertz, W.R. 2006. KCNE1 subunits require co-assembly with K+ channels for efficient trafficking and cell surface expression. *J Biol Chem*. 281:40015-40023.

Chen, H. and Goldstein, S.A. 2007. Serial perturbation of MinK in IKs implies an alpha-helical transmembrane span traversing the channel corpus. *Biophys J*. 93:2332-2340.

Chen, H., Kim, L.A., Rajan, S., Xu, S. and Goldstein, S.A. 2003a. Charybdotoxin binding in the I(Ks) pore demonstrates two MinK subunits in each channel complex. *Neuron*. 40:15-23.

Chen, H., Sesti, F. and Goldstein, S.A. 2003b. Pore- and state-dependent cadmium block of I(Ks) channels formed with MinK-55C and wild-type KCNQ1 subunits. *Biophys J*. 84:3679-3689.

Choi, K.L., Mossman, C., Aube, J. and Yellen, G. 1993. The internal quaternary ammonium receptor site of Shaker potassium channels. *Neuron*. 10:533-541.

Creighton, T.E. 1992. Proteins: Structures and Molecular Properties. Vol. 2nd ed. edition. W. H. Freeman and Company, New York, NY, 512 pp.

Darman, R.B., Ivy, A.A., Ketty, V. and Blaustein, R.O. 2006. Constraints on voltage sensor movement in the shaker K+ channel. *J Gen Physiol*. 128:687-699.

del Camino, D., Holmgren, M., Liu, Y. and Yellen, G. 2000. Blocker protection in the pore of a voltage-gated K+ channel and its structural implications. *Nature*. 403:321-325.

del Camino, D. and Yellen, G. 2001. Tight steric closure at the intracellular activation gate of a voltage-gated K(+) channel. *Neuron*. 32:649-656.

Doyle, D.A., Morais Cabral, J., Pfuetzner, R.A., Kuo, A., Gulbis, J.M., Cohen, S.L., Chait, B.T. and MacKinnon, R. 1998. The structure of the potassium channel: molecular basis of K+ conduction and selectivity. *Science*. 280:69-77.

Gage, S.D. 2008. Structural and Functional Studies of the KCNQ1-KCNE K+ Channel Complex. , University of Massachusetts Medical School, Worcester, MA.

Gage, S.D. and Kobertz, W.R. 2004. KCNE3 Truncation Mutants Reveal a Bipartite Modulation of KCNQ1 K+ Channels. *J. Gen. Physiol.* 124:759-771.

Ghosh, S., Nunziato, D.A. and Pitt, G.S. 2006. KCNQ1 assembly and function is blocked by long-QT syndrome mutations that disrupt interaction with calmodulin. *Circ Res*. 98:1048-1054.

Grunnet, M., Jespersen, T., Rasmussen, H.B., Ljungstrom, T., Jorgensen, N.K., Olesen, S.P. and Klaerke, D.A. 2002. KCNE4 is an inhibitory subunit to the KCNQ1 channel. *J Physiol*. 542:119-130.

Hayashi, N., Matsubara, M., Takasaki, A., Titani, K. and Taniguchi, H. 1998. An expression system of rat calmodulin using T7 phage promoter in Escherichia coli. *Protein Expr Purif*. 12:25-28.

Hodgkin, A.L. and Huxley, A.F. 1952. A quantitative description of membrane current and its application to conduction and excitation in nerve. *J Physiol*. 117:500-544.

Holmgren, M., Shin, K.S. and Yellen, G. 1998. The activation gate of a voltage-gated K+ channel can be trapped in the open state by an intersubunit metal bridge. *Neuron*. 21:617-621.

Hong, K.H. and Miller, C. 2000. The lipid-protein interface of a Shaker K(+) channel. *J Gen Physiol*. 115:51-58.

Hoshi, T., Zagotta, W.N. and Aldrich, R.W. 1990. Biophysical and molecular mechanisms of Shaker potassium channel inactivation. *Science*. 250:533-538.

Howard, R.J., Clark, K.A., Holton, J.M. and Minor, D.L., Jr. 2007. Structural insight into KCNQ (Kv7) channel assembly and channelopathy. *Neuron*. 53:663-675.

Islas, L.D. and Sigworth, F.J. 1999. Voltage sensitivity and gating charge in Shaker and Shab family potassium channels. *J Gen Physiol*. 114:723-742.

Jervell, A. and Lange-Nielsen, F. 1957. Congenital deaf-mutism, functional heart disease with prolongation of the Q-T interval and sudden death. *Am Heart J*. 54:59-68.

Jiang, Y., Lee, A., Chen, J., Cadene, M., Chait, B.T. and MacKinnon, R. 2002a. Crystal structure and mechanism of a calcium-gated potassium channel. *Nature*. 417:515-522.

Jiang, Y., Lee, A., Chen, J., Cadene, M., Chait, B.T. and MacKinnon, R. 2002b. The open pore conformation of potassium channels. *Nature*. 417:523-526.

Jiang, Y., Lee, A., Chen, J., Ruta, V., Cadene, M., Chait, B.T. and MacKinnon, R. 2003a. X-ray structure of a voltage-dependent K+ channel. *Nature*. 423:33-41.

Jiang, Y., Ruta, V., Chen, J., Lee, A. and MacKinnon, R. 2003b. The principle of gating charge movement in a voltage-dependent K+ channel. *Nature*. 423:42-48.

Kang, C., Tian, C., Sonnichsen, F.D., Smith, J.A., Meiler, J., George, A.L., Jr., Vanoye, C.G., Kim, H.J. and Sanders, C.R. 2008. Structure of KCNE1 and implications for how it modulates the KCNQ1 potassium channel. *Biochemistry*. 47:7999-8006.

Karlin, A. and Akabas, M.H. 1998. Substituted-cysteine accessibility method. *Methods Enzymol*. 293:123-145.

Kass, R.S. and Moss, A.J. 2003. Long QT syndrome: novel insights into the mechanisms of cardiac arrhythmias. *J Clin Invest*. 112:810-815.

Kass, R.S. and Wiegers, S.E. 1982. The ionic basis of concentration-related effects of noradrenaline on the action potential of calf cardiac purkinje fibres. *J Physiol*. 322:541-558.

Kurokawa, J., Chen, L. and Kass, R.S. 2003. Requirement of subunit expression for cAMP-mediated regulation of a heart potassium channel. *Proc Natl Acad Sci U S A*. 100:2122-2127.

Kwon, Y., Hofmann, T. and Montell, C. 2007. Integration of phosphoinositide- and calmodulin-mediated regulation of TRPC6. *Mol Cell*. 25:491-503.

Lai, L.P., Su, Y.N., Hsieh, F.J., Chiang, F.T., Juang, J.M., Liu, Y.B., Ho, Y.L., Chen, W.J., Yeh, S.J., Wang, C.C., Ko, Y.L., Wu, T.J., Ueng, K.C., Lei, M.H., Tsao, H.M., Chen, S.A., Lin, T.K., Wu, M.H., Lo, H.M., Huang, S.K. and Lin, J.L. 2005. Denaturing high-performance liquid chromatography screening of the long QT syndrome-related cardiac sodium and potassium channel genes and identification of novel mutations and single nucleotide polymorphisms. *J Hum Genet*. 50:490-496.

Larsson, H.P., Baker, O.S., Dhillon, D.S. and Isacoff, E.Y. 1996. Transmembrane movement of the shaker K+ channel S4. *Neuron*. 16:387-397.

Letts, V.A., Valenzuela, A., Dunbar, C., Zheng, Q.Y., Johnson, K.R. and Frankel, W.N. 2000. A new spontaneous mouse mutation in the Kcne1 gene. *Mamm Genome*. 11:831-835.

Li-Smerin, Y., Hackos, D.H. and Swartz, K.J. 2000a. alpha-helical structural elements within the voltage-sensing domains of a K(+) channel. *J Gen Physiol*. 115:33-50.

Li-Smerin, Y., Hackos, D.H. and Swartz, K.J. 2000b. A localized interaction surface for voltage-sensing domains on the pore domain of a K+ channel. *Neuron*. 25:411-423.

Liu, Y., Holmgren, M., Jurman, M.E. and Yellen, G. 1997. Gated access to the pore of a voltage-dependent K+ channel. *Neuron*. 19:175-184.

Long, S.B., Campbell, E.B. and Mackinnon, R. 2005a. Crystal structure of a mammalian voltage-dependent Shaker family K+ channel. *Science*. 309:897-903.

Long, S.B., Campbell, E.B. and Mackinnon, R. 2005b. Voltage sensor of Kv1.2: structural basis of electromechanical coupling. *Science*. 309:903-908.

Long, S.B., Tao, X., Campbell, E.B. and MacKinnon, R. 2007. Atomic structure of a voltage-dependent K+ channel in a lipid membrane-like environment. *Nature*. 450:376-382.

Lopez-Barneo, J., Hoshi, T., Heinemann, S.H. and Aldrich, R.W. 1993. Effects of external cations and mutations in the pore region on C-type inactivation of Shaker potassium channels. *Receptors Channels*. 1:61-71.

Loussouarn, G. and Escande, D. 2003. Functional KCNQ1/KCNE1 channel complex requires both intracellular PIP2 and MgATP. *Biophysical Society Abstract*.

Lu, Z., Klem, A.M. and Ramu, Y. 2001. Ion conduction pore is conserved among potassium channels. *Nature*. 413:809-813.

Lu, Z., Klem, A.M. and Ramu, Y. 2002. Coupling between voltage sensors and activation gate in voltage-gated K+ channels. *J Gen Physiol*. 120:663-676.

Lundquist, A.L., Manderfield, L.J., Vanoye, C.G., Rogers, C.S., Donahue, B.S., Chang, P.A., Drinkwater, D.C., Murray, K.T. and George, A.L., Jr. 2005. Expression of multiple KCNE genes in human heart may enable variable modulation of I(Ks). *J Mol Cell Cardiol*. 38:277-287.

Ma, L., Lin, C., Teng, S., Chai, Y., Bahring, R., Vardanyan, V., Li, L., Pongs, O. and Hui, R. 2003. Characterization of a novel Long QT syndrome mutation G52R-KCNE1 in a Chinese family. *Cardiovasc Res*. 59:612-619.

MacKinnon, R. 1991. Determination of the subunit stoichiometry of a voltage-activated potassium channel. *Nature*. 350:232-235.

Maduke, M., Williams, C. and Miller, C. 1998. Formation of CLC-0 chloride channels from separated transmembrane and cytoplasmic domains. *Biochemistry*. 37:1315-1321.

Manderfield, L.J., Daniels, M.A., Vanoye, C.G. and George, A.L., Jr. 2008. 1811-Plat Structural Determinants for KCNE4 Inhibition of KCNQ1. *Biophys. J.* 94:1811-.

Manderfield, L.J. and George, A.L., Jr. 2008. KCNE4 can co-associate with the I(Ks) (KCNQ1-KCNE1) channel complex. *Febs J*. 275:1336-1349.

Mannikko, R., Elinder, F. and Larsson, H.P. 2002. Voltage-sensing mechanism is conserved among ion channels gated by opposite voltages. *Nature*. 419:837-841.

Marx, S.O., Kurokawa, J., Reiken, S., Motoike, H., D'Armiento, J., Marks, A.R. and Kass, R.S. 2002. Requirement of a macromolecular signaling complex for beta adrenergic receptor modulation of the KCNQ1-KCNE1 potassium channel. *Science*. 295:496-499.

McCrossan, Z.A. and Abbott, G.W. 2004. The MinK-related peptides. *Neuropharmacology*. 47:787-821.

Melman, Y.F., Domenech, A., de la Luna, S. and McDonald, T.V. 2001. Structural determinants of KvLQT1 control by the KCNE family of proteins. *J Biol Chem*. 276:6439-6444.

Melman, Y.F., Krumerman, A. and McDonald, T.V. 2002. A single transmembrane site in the KCNE-encoded proteins controls the specificity of KvLQT1 channel gating. *J Biol Chem*. 277:25187-25194.

Melman, Y.F., Um, S.Y., Krumerman, A., Kagan, A. and McDonald, T.V. 2004. KCNE1 Binds to the KCNQ1 Pore to Regulate Potassium Channel Activity. *Neuron*. 42:927-937.

Monks, S.A., Needleman, D.J. and Miller, C. 1999. Helical structure and packing orientation of the S2 segment in the Shaker K+ channel. *J Gen Physiol*. 113:415-423.

Morais-Cabral, J.H., Zhou, Y. and MacKinnon, R. 2001. Energetic optimization of ion conduction rate by the K+ selectivity filter. *Nature*. 414:37-42.

Morin, T.J. and Kobertz, W.R. 2007. A derivatized scorpion toxin reveals the functional output of heteromeric KCNQ1-KCNE K+ channel complexes. *ACS Chem Biol*. 2:469-473.

Morin, T.J. and Kobertz, W.R. 2008. Counting membrane-embedded KCNE beta-subunits in functioning K+ channel complexes. *Proc Natl Acad Sci U S A*. 105:1478-1482.

Murata, Y., Iwasaki, H., Sasaki, M., Inaba, K. and Okamura, Y. 2005. Phosphoinositide phosphatase activity coupled to an intrinsic voltage sensor. *Nature*. 435:1239-1243.

Nakajo, K. and Kubo, Y. 2007. KCNE1 and KCNE3 stabilize and/or slow voltage sensing S4 segment of KCNQ1 channel. *J Gen Physiol*. 130:269-281.

Napolitano, C., Priori, S.G., Schwartz, P.J., Bloise, R., Ronchetti, E., Nastoli, J., Bottelli, G., Cerrone, M. and Leonardi, S. 2005. Genetic testing in the long QT syndrome: development and validation of an efficient approach to genotyping in clinical practice. *Jama*. 294:2975-2980.

Nicolas, C.S., Park, K.H., El Harchi, A., Camonis, J., Kass, R.S., Escande, D., Merot, J., Loussouarn, G., Le Bouffant, F. and Baro, I. 2008. IKs response to protein kinase A-dependent KCNQ1 phosphorylation requires direct interaction with microtubules. *Cardiovasc Res*. 79:427-435.

Nishikawa, K., Toker, A., Johannes, F.J., Songyang, Z. and Cantley, L.C. 1997. Determination of the specific substrate sequence motifs of protein kinase C isozymes. *J Biol Chem*. 272:952-960.

Panaghie, G. and Abbott, G.W. 2007. The role of S4 charges in voltage-dependent and voltage-independent KCNQ1 potassium channel complexes. *J Gen Physiol*. 129:121-133.

Panaghie, G., Tai, K.K. and Abbott, G.W. 2006. Interaction of KCNE subunits with the KCNQ1 K+ channel pore. *J Physiol*. 570:455-467.

Phillips, L.R., Milescu, M., Li-Smerin, Y., Mindell, J.A., Kim, J.I. and Swartz, K.J. 2005. Voltage-sensor activation with a tarantula toxin as cargo. *Nature*. 436:857-860.

Posson, D.J., Ge, P., Miller, C., Bezanilla, F. and Selvin, P.R. 2005. Small vertical movement of a K+ channel voltage sensor measured with luminescence energy transfer. *Nature*. 436:848-851.

Pusch, M. 1998. Increase of the single-channel conductance of KvLQT1 potassium channels induced by the association with minK. *Pflugers Arch*. 437:172-174.

Pusch, M., Magrassi, R., Wollnik, B. and Conti, F. 1998. Activation and inactivation of homomeric KvLQT1 potassium channels. *Biophys J*. 75:785-792.

Ramsey, I.S., Moran, M.M., Chong, J.A. and Clapham, D.E. 2006. A voltage-gated proton-selective channel lacking the pore domain. *Nature*. 440:1213-1216.

Rees, D.C., Komiya, H., Yeates, T.O., Allen, J.P. and Feher, G. 1989. The bacterial photosynthetic reaction center as a model for membrane proteins. *Annu Rev Biochem*. 58:607-633.

Robbins, J. 2001. KCNQ potassium channels: physiology, pathophysiology, and pharmacology. *Pharmacol Ther*. 90:1-19.

Roepke, T.K., Anantharam, A., Kirchhoff, P., Busque, S.M., Young, J.B., Geibel, J.P., Lerner, D.J. and Abbott, G.W. 2006. The KCNE2 potassium channel ancillary subunit is essential for gastric acid secretion. *J Biol Chem*. 281:23740-23747.

Rohl, C.A., Chakrabartty, A. and Baldwin, R.L. 1996. Helix propagation and N-cap propensities of the amino acids measured in alanine-based peptides in 40 volume percent trifluoroethanol. *Protein Sci*. 5:2623-2637.

Romano, C., Gemme, G. and Pongiglione, R. 1963. [Rare Cardiac Arrythmias of the Pediatric Age. Ii. Syncopal Attacks Due to Paroxysmal Ventricular Fibrillation. (Presentation of 1st Case in Italian Pediatric Literature)]. *Clin Pediatr (Bologna)*. 45:656-683.

Rosen, H. 1957. A modified ninhydrin colorimetric analysis for amino acids. *Arch Biochem Biophys*. 67:10-15.

Ruta, V., Chen, J. and MacKinnon, R. 2005. Calibrated measurement of gating-charge arginine displacement in the KvAP voltage-dependent K+ channel. *Cell*. 123:463-475.

Ruta, V., Jiang, Y., Lee, A., Chen, J. and MacKinnon, R. 2003. Functional analysis of an archaebacterial voltage-dependent K+ channel. *Nature*. 422:180-185.

Sanguinetti, M.C., Curran, M.E., Zou, A., Shen, J., Spector, P.S., Atkinson, D.L. and Keating, M.T. 1996. Coassembly of K(V)LQT1 and minK (IsK) proteins to form cardiac I(Ks) potassium channel. *Nature*. 384:80-83.

Sasaki, M., Takagi, M. and Okamura, Y. 2006. A voltage sensor-domain protein is a voltage-gated proton channel. *Science*. 312:589-592.

Schroeder, B.C., Waldegger, S., Fehr, S., Bleich, M., Warth, R., Greger, R. and Jentsch, T.J. 2000. A constitutively open potassium channel formed by KCNQ1 and KCNE3. *Nature*. 403:196-199.

Schulze-Bahr, E., Schwarz, M., Hauenschild, S., Wedekind, H., Funke, H., Haverkamp, W., Breithardt, G., Pongs, O. and Isbrandt, D. 2001. A novel long-QT 5 gene mutation in the C-terminus (V109I) is associated with a mild phenotype. *J Mol Med*. 79:504-509.

Schwartz, P.J., Priori, S.G., Spazzolini, C., Moss, A.J., Vincent, G.M., Napolitano, C., Denjoy, I., Guicheney, P., Breithardt, G., Keating, M.T., Towbin, J.A., Beggs, A.H., Brink, P., Wilde, A.A., Toivonen, L., Zareba, W., Robinson, J.L., Timothy, K.W., Corfield, V., Wattanasirichaigoon, D., Corbett, C., Haverkamp, W., Schulze-Bahr, E., Lehmann, M.H., Schwartz, K., Coumel, P. and Bloise, R. 2001. Genotype-phenotype correlation in the long-QT syndrome: gene-specific triggers for life-threatening arrhythmias. *Circulation*. 103:89-95.

Seoh, S.A., Sigg, D., Papazian, D.M. and Bezanilla, F. 1996. Voltage-sensing residues in the S2 and S4 segments of the Shaker K+ channel. *Neuron*. 16:1159-1167.

Sesti, F. and Goldstein, S.A. 1998. Single-channel characteristics of wild-type IKs channels and channels formed with two minK mutants that cause long QT syndrome. *J Gen Physiol*. 112:651-663.

Shamgar, L., Ma, L., Schmitt, N., Haitin, Y., Peretz, A., Wiener, R., Hirsch, J., Pongs, O. and Attali, B. 2006. Calmodulin is essential for cardiac IKS channel gating and assembly: impaired function in long-QT mutations. *Circ Res*. 98:1055-1063.

Soler-Llavina, G.J., Chang, T.H. and Swartz, K.J. 2006. Functional interactions at the interface between voltage-sensing and pore domains in the Shaker K(v) channel. *Neuron*. 52:623-634.

Splawski, I., Shen, J., Timothy, K.W., Lehmann, M.H., Priori, S., Robinson, J.L., Moss, A.J., Schwartz, P.J., Towbin, J.A., Vincent, G.M. and Keating, M.T. 2000. Spectrum of mutations in long-QT syndrome genes. KVLQT1, HERG, SCN5A, KCNE1, and KCNE2. *Circulation*. 102:1178-1185.

Splawski, I., Tristani-Firouzi, M., Lehmann, M.H., Sanguinetti, M.C. and Keating, M.T. 1997. Mutations in the hminK gene cause long QT syndrome and suppress IKs function. *Nat Genet*. 17:338-340.

Starace, D.M. and Bezanilla, F. 2004. A proton pore in a potassium channel voltage sensor reveals a focused electric field. *Nature*. 427:548-553.

Starace, D.M., Stefani, E. and Bezanilla, F. 1997. Voltage-dependent proton transport by the voltage sensor of the Shaker K+ channel. *Neuron*. 19:1319-1327.

Stauffer, D.A. and Karlin, A. 1994. Electrostatic potential of the acetylcholine binding sites in the nicotinic receptor probed by reactions of binding-site cysteines with charged methanethiosulfonates. *Biochemistry*. 33:6840-6849.

Sukhareva, M., Hackos, D.H. and Swartz, K.J. 2003. Constitutive activation of the Shaker Kv channel. *J Gen Physiol*. 122:541-556.

Tai, K.K. and Goldstein, S.A. 1998. The conduction pore of a cardiac potassium channel. *Nature*. 391:605-608.

Takumi, T., Moriyoshi, K., Aramori, I., Ishii, T., Oiki, S., Okada, Y., Ohkubo, H. and Nakanishi, S. 1991. Alteration of channel activities and gating by mutations of slow ISK potassium channel. *J Biol Chem*. 266:22192-22198.

Takumi, T., Ohkubo, H. and Nakanishi, S. 1988. Cloning of a membrane protein that induces a slow voltage-gated potassium current. *Science*. 242:1042-1045.

Tapper, A.R. and George, A.L., Jr. 2000. MinK subdomains that mediate modulation of and association with KvLQT1. *J Gen Physiol*. 116:379-390.

Tapper, A.R. and George, A.L., Jr. 2001. Location and orientation of minK within the I(Ks) potassium channel complex. *J Biol Chem*. 276:38249-38254.

Tinel, N., Diochot, S., Borsotto, M., Lazdunski, M. and Barhanin, J. 2000. KCNE2 confers background current characteristics to the cardiac KCNQ1 potassium channel. *Embo J*. 19:6326-6330.

Tombola, F., Pathak, M.M. and Isacoff, E.Y. 2006. How does voltage open an ion channel? *Annu Rev Cell Dev Biol*. 22:23-52.

Tu, L. and Deutsch, C. 1999. Evidence for dimerization of dimers in K+ channel assembly. *Biophys J*. 76:2004-2017.

Vemana, S., Pandey, S. and Larsson, H.P. 2004. S4 movement in a mammalian HCN channel. *J Gen Physiol*. 123:21-32.

Wang, K.W. and Goldstein, S.A. 1995. Subunit composition of minK potassium channels. *Neuron*. 14:1303-1309.

Wang, Q., Curran, M.E., Splawski, I., Burn, T.C., Millholland, J.M., VanRaay, T.J., Shen, J., Timothy, K.W., Vincent, G.M., de Jager, T., Schwartz, P.J., Toubin, J.A., Moss, A.J., Atkinson, D.L., Landes, G.M., Connors, T.D. and Keating, M.T. 1996. Positional cloning of a novel potassium channel gene: KVLQT1 mutations cause cardiac arrhythmias. *Nat Genet*. 12:17-23.

Wang, W., Xia, J. and Kass, R.S. 1998. MinK-KvLQT1 fusion proteins, evidence for multiple stoichiometries of the assembled IsK channel. *J Biol Chem*. 273:34069-34074.

Wangemann, P., Liu, J. and Marcus, D.C. 1995. Ion transport mechanisms responsible for K+ secretion and the transepithelial voltage across marginal cells of stria vascularis in vitro. *Hear Res*. 84:19-29.

Ward, O.C. 1964. A New Familial Cardiac Syndrome in Children. *J Ir Med Assoc*. 54:103-106.

Webster, S.M., Del Camino, D., Dekker, J.P. and Yellen, G. 2004. Intracellular gate opening in Shaker K+ channels defined by high-affinity metal bridges. *Nature*. 428:864-868.

Wiener, R., Haitin, Y., Shamgar, L., Fernandez-Alonso, M.C., Martos, A., Chomsky-Hecht, O., Rivas, G., Attali, B. and Hirsch, J.A. 2008. The KCNQ1 (Kv7.1) COOH terminus, a multitiered scaffold for subunit assembly and protein interaction. *J Biol Chem*. 283:5815-5830.

Wilson, A.J., Quinn, K.V., Graves, F.M., Bitner-Glindzicz, M. and Tinker, A. 2005. Abnormal KCNQ1 trafficking influences disease pathogenesis in hereditary long QT syndromes (LQT1). *Cardiovasc Res*. 67:476-486.

Xu, X., Jiang, M., Hsu, K.L., Zhang, M. and Tseng, G.N. 2008. KCNQ1 and KCNE1 in the IKs channel complex make state-dependent contacts in their extracellular domains. *J Gen Physiol*. 131:589-603.

Yang, N., George, A.L., Jr. and Horn, R. 1996. Molecular basis of charge movement in voltage-gated sodium channels. *Neuron*. 16:113-122.

Yang, N. and Horn, R. 1995. Evidence for voltage-dependent S4 movement in sodium channels. *Neuron*. 15:213-218.

Yang, W.P., Levesque, P.C., Little, W.A., Conder, M.L., Shalaby, F.Y. and Blanar, M.A. 1997. KvLQT1, a voltage-gated potassium channel responsible for human cardiac arrhythmias. *Proc Natl Acad Sci U S A*. 94:4017-4021.

Yang, Y. and Sigworth, F.J. 1998. Single-channel properties of IKs potassium channels. *J Gen Physiol*. 112:665-678.

Yellen, G. 1998. The moving parts of voltage-gated ion channels. *Q Rev Biophys*. 31:239-295.

Yohannan, S., Faham, S., Yang, D., Whitelegge, J.P. and Bowie, J.U. 2004. The evolution of transmembrane helix kinks and the structural diversity of G protein-coupled receptors. *Proc Natl Acad Sci U S A*. 101:959-963.

Yus-Najera, E., Santana-Castro, I. and Villarroel, A. 2002. The identification and characterization of a noncontinuous calmodulin-binding site in noninactivating voltage-dependent KCNQ potassium channels. *J Biol Chem*. 277:28545-28553.

Yusaf, S.P., Wray, D. and Sivaprasadarao, A. 1996. Measurement of the movement of the S4 segment during the activation of a voltage-gated potassium channel. *Pflugers Arch*. 433:91-97.

Zagotta, W.N., Hoshi, T. and Aldrich, R.W. 1990. Restoration of inactivation in mutants of Shaker potassium channels by a peptide derived from ShB. *Science*. 250:568-571.

Zerangue, N., Schwappach, B., Jan, Y.N. and Jan, L.Y. 1999. A new ER trafficking signal regulates the subunit stoichiometry of plasma membrane K(ATP) channels. *Neuron*. 22:537-548.

Zhou, Y., Morais-Cabral, J.H., Kaufman, A. and MacKinnon, R. 2001. Chemistry of ion coordination and hydration revealed by a K+ channel-Fab complex at 2.0 A resolution. *Nature*. 414:43-48.